NAVAL POSTGRADUATE SCHOOL

MONTEREY, CALIFORNIA

THESIS

SYNTHESIS AND CHARACTERIZATION OF ALUMINUM-CARBON NANOTUBE COMPOSITE POWDERS BY CRYOGENIC MILLING

by

Brent A. Bottolfson

March 2012

Thesis Co-Advisors: Sebastian Osswald
Luke Brewer

Approved for public release; distribution is unlimited

THIS PAGE INTENTIONALLY LEFT BLANK

REPORT DOCUMENTATION PAGE		Form Approved OMB No. 0704-0188

1. AGENCY USE ONLY *(Leave blank)*	2. REPORT DATE March 2012	3. REPORT TYPE AND DATES COVERED Master's Thesis

4. TITLE AND SUBTITLE Synthesis and Characterization of Aluminum-Carbon Nanotube Composite by Cryogenic Milling	5. FUNDING NUMBERS
6. AUTHOR(S) Brent A. Bottolfson	
7. PERFORMING ORGANIZATION NAME(S) AND ADDRESS(ES) Naval Postgraduate School Monterey, CA 93943-5000	8. PERFORMING ORGANIZATION REPORT NUMBER
9. SPONSORING /MONITORING AGENCY NAME(S) AND ADDRESS(ES) N/A	10. SPONSORING/MONITORING AGENCY REPORT NUMBER

11. SUPPLEMENTARY NOTES The views expressed in this thesis are those of the author and do not reflect the official policy or position of the Department of Defense or the U.S. Government. IRB Protocol number _____N/A_____.

12a. DISTRIBUTION / AVAILABILITY STATEMENT Approved for public release; distribution is unlimited	12b. DISTRIBUTION CODE A

13. ABSTRACT (maximum 200 words)

Cryogenic milling was studied for the ex situ strengthening of aluminum (Al) with carbon nanotubes (CNT). Characterization of mechanically alloyed Al-CNT powders was conducted in preparation for bulk powder processing to be used in cold spray. Al-CNT metal matrix composite powders with 5 wt.% and 10 wt.% CNT were synthesized by cryogenic milling of the blended component powders. Stearic acid was used as a process control agent to minimize agglomeration of the powders upon milling. CNT reinforcement of the Al powder was successfully obtained while maintain CNT structure after milling the powders for periods ranging between six and 90 minutes using a SPEX 6870 Freezer/Mill. Composition and properties of the Al-CNT composite was studied using X-ray diffraction, optical microscopy, nanoindentation, scanning electron microscopy (SEM), Raman spectroscopy, and laser diffraction particle size analysis.

14. SUBJECT TERMS Aluminum. Carbon Nanotube, Composite, Cryogenic Milling, Mechanical Alloying, Metal Matrix	15. NUMBER OF PAGES 75
	16. PRICE CODE

17. SECURITY CLASSIFICATION OF REPORT	18. SECURITY CLASSIFICATION OF THIS PAGE	19. SECURITY CLASSIFICATION OF ABSTRACT	20. LIMITATION OF ABSTRACT
Unclassified	Unclassified	Unclassified	UU

NSN 7540-01-280-5500

Standard Form 298 (Rev. 2-89)
Prescribed by ANSI Std. 239-18

THIS PAGE INTENTIONALLY LEFT BLANK

Approved for public release; distribution is unlimited

SYNTHESIS AND CHARACTERIZATION OF ALUMINUM-CARBON NANOTUBE COMPOSITE POWDERS BY CRYOGENIC MILLING

Brent A. Bottolfson
Lieutenant, United States Navy
B.S., University of Idaho, 2005

Submitted in partial fulfillment of the
requirements for the degree of

MASTER OF SCIENCE IN MECHANICAL ENGINEERING

from the

NAVAL POSTGRADUATE SCHOOL
March 2012

Author: Brent A. Bottolfson

Approved by: Sebastian Osswald
Thesis Co-Advisor

Luke Brewer
Thesis Co-Advisor

Knox Millsaps
Chair, Department of Mechanical and Aerospace Engineering

THIS PAGE INTENTIONALLY LEFT BLANK

ABSTRACT

Cryogenic milling was studied for the ex situ strengthening of aluminum (Al) with carbon nanotubes (CNT). Characterization of mechanically alloyed Al-CNT powders was conducted in preparation for bulk powder processing to be used in cold spray. Al-CNT metal matrix composite powders with 5 wt.% and 10 wt.% CNT were synthesized by cryogenic milling of the blended component powders. Stearic acid was used as a process control agent to minimize agglomeration of the powders upon milling. CNT reinforcement of the Al powder was successfully obtained while maintaining CNT structure after milling the powders for periods ranging between six and 90 minutes using a SPEX 6870 Freezer/Mill. Composition and properties of the Al-CNT composite was studied using X-ray diffraction, optical microscopy, nanoindentation, scanning electron microscopy (SEM), Raman spectroscopy, and laser diffraction particle size analysis.

THIS PAGE INTENTIONALLY LEFT BLANK

TABLE OF CONTENTS

THIS PAGE INTENTIONALLY LEFT BLANK

LIST OF FIGURES

THIS PAGE INTENTIONALLY LEFT BLANK

LIST OF TABLES

THIS PAGE INTENTIONALLY LEFT BLANK

LIST OF ACRONYMS AND ABBREVIATIONS

Al	Aluminum
Ar	Argon
BPR	Ball to Powder Ratio
CNT	Carbon Nanotube
Cu	Copper
CS	Cold Spray
EFP	Explosively Formed Penetrator
FCC	Face Centered Cubic
FWHM	Full Width Half Maximum
HP	Hot Pressing
IED	Improvised Explosive Device
LN	Liquid Nitrogen
MA	Mechanical Alloying
MM	Metal Matrix
MMC	Metal Matrix Composite
MRAP	Mine Resistant Ambush Protected Vehicle
MWCNT	Multiwalled Carbon Nanotube
nm	Nanometer
ND	Nanodiamond
PCA	Process Control Agent
P-V	Pseudo-Voight
SEM	Scanning Electron Microscopy
TEM	Transmission Electron Microscopy
vol.	Volume
W-H	Williamson-Hall
wt.	Weight
XRD	X-ray Diffraction

THIS PAGE INTENTIONALLY LEFT BLANK

LIST OF SYMBOLS

τ_a	Resolved shear stress
τ_o	Friction stress
τ_c	Critical stress
k	Hall-Petch slope
r	Distance from a Frank-Read source to a grain boundary
b	Burgers vector
G	Shear modulus
E	Young's modulus
V_f	Volume fraction
θ	Diffraction angle
S	Stiffness
A	Projected area of contact
H	Hardness
P_{max}	Maximum indentation load
β	Total broadening
η	Shape factor
Γ	Observed broadening

THIS PAGE INTENTIONALLY LEFT BLANK

ACKNOWLEDGMENTS

I would first like to thank my thesis advisor, Dr. Sebastian Osswald. Thank you for countless hours you have invested in this project. I appreciate your dedication and willingness to be available, teach, and assist me with this project.

Secondly, I thank my co-advisor, Dr. Luke Brewer. He has always been available and has always helped to find a solution when I have had questions or needed assistance. Your guidance on this project is equally appreciated.

Third, Dr. Sarath Menon has helped tremendously with the lab equipment and analysis of XRD data. As the other professors, he has always gone out of his way to make certain I had a solution to any issues I encountered.

Last, a special thank you to Alex McGinnis for both teaching me how to use the lab equipment and being a "weekend warrior" over several quarters to complete class projects.

THIS PAGE INTENTIONALLY LEFT BLANK

I. INTRODUCTION

A. MOTIVATION FOR LIGHTWEIGHT ARMOR

The development of stronger and more lightweight armor materials is of key importance to the success of the United States military in both the Global War on Terrorism and the war in Afghanistan. Improvised Explosive Devices (IED) have become a common tactic of our enemies, causing numerous deaths and injuries to our forces and allies. Since World War II, armored vehicles have gone through multiple generations of armor development to increase protection of passengers from explosions. Early generations included sandbags belted to the floor of the vehicle for increased vehicle mass, followed by blast deflectors in wheel arches, and later mine resistant V-shaped hulls [1]. These methods all add mass to the already heavy and cumbersome vehicles. The US military has spent billions of dollars on the Mine Resistant Ambush Protected Vehicle (MRAP) for use in the Middle East. While MRAPs are much more effective against roadside bombs, they show particular weakness to Explosively Formed Penetrators (EFP). The controversial MRAP program has come under scrutiny because of insufficient side armor that is not resistant to EFPs. In 2005, Marine Corps Commanders requested 3400 sets of additional armor to be used on these vehicles for EFP protection. Even this add-on armor is not expected to fully stop damage due to the ability of EFPs to penetrate existing armor by use of a metal-capped slug over the explosive charge [2]. Maintaining resistance to blasts from IEDs, EFPs, and small arms fire while keeping these vehicles both as lightweight as possible and maneuverable is essential to success in counter insurgent missions.

Armors used for personal protection are commonly made of polymer based composite fiber materials such as Kevlar. While development of these body armors has greatly improved survivability in combat, they still have some shortcomings. Multiple layers of these composites can become bulky and stiff on the wearer, limiting movement of the wearer's joints. Development of lighter, more flexible, and more impact resistant materials for use in body armor is fundamentally important for the protection of US troops in combat.

In both cases of vehicle and personal armor materials, the challenge is to find materials with a combination of material properties that can provide the best protection from projectile impacts. Hard material properties are desirable for such application, but as materials become harder they typically are more brittle and prone to fracture. On the contrary, materials for such armor also need to have tough and ductile properties. Due to their exceptional mechanical properties, carbon nanomaterials, particularly carbon nanotubes (CNT) and nanodiamond (ND) have successfully been used to reinforce polymers. CNTs are the strongest fibers known to man while ND is considered one of the hardest naturally occurring materials. The reinforcement of a lightweight, ductile metal with carbon nanomaterials could therefore provide a material that offers superior mechanical properties and fragment resistance as compared to conventional carbon fiber- or ceramic fiber-reinforced metals while maintaining a weight similar to that of reinforced polymer armors [3], [4]. Unfortunately, until recently, research of nano-scale reinforced armor materials has been primarily focused on polymer-based materials. Far less work has been conducted on the nano-scale reinforcement of metals. A 10-year analysis between 1997 and 2007 of publications of polymer, ceramic, and metal matrix composites shows that polymer research far outweighs that of metal composites by about 10:1 [5]. This is due to the ease of manufacture and processing of polymers. Metal reinforced composites are not easily manufactured or processed such that the integrity of the reinforcement is preserved. Cold spray technology (CS) is a promising processing method for nano-carbon reinforced metal powders. LT Brian Sneed's thesis was a study of aluminum (AL)-ND based composites; this focus of this study is Al-CNT based composites [6].

B. METAL MATRIX COMPOSITES

1. Reinforcement through Powder Processing

Metal Matrix Composites (MMC) are combinations of a metal matrix (MM) which provides metallic properties of ductility and toughness with a reinforcement component that provides ceramic properties of high strength and high modulus [7]. The reinforcements used in MMCs can be in the form of particles or fibers [7]. Powder metallurgy is the preferred method of processing MMCs containing CNTs. Processing of

MM-CNT composites is necessary to attain homogeneous dispersion of CNTs, strong bond strength between the MM and CNTs, and chemical and structural stability of the CNTs [5]. Powder metallurgy is an excellent means for MM reinforcement through dispersion strengthening. CNT based composites can have problems with CNT agglomeration and poor distribution/dispersion within a MM due to many factors such as: the orientation of CNTs, homogeneity, nanotube matrix adhesion, nanotube aspect ratio, and the volume fraction of nanotubes [8]. But, by tailoring the milling conditions, parameters, and CNT content in the MM these problems may be resolved.

2. Strengthening by Reduction of Grain Size

A reduction of grain size is often used to strengthen metals of crystalline structure; nanocrystalline materials with grain sizes of 100 nm and below are known to be high-strength materials [9]. This method of strengthening limits movement of dislocations through grains. Hall-Petch, Cottrell, and Li theories all show an inverse dependence on grain size, where *D* is the grain diameter. The Hall-Petch theory is based on the observation that grain boundaries will hinder dislocation movement. By having smaller grain size, dislocations are less able to traverse between grain boundaries. The Cottrell theory is similar in that dislocations are less likely to traverse grains, the difference being that solute atoms in the lattice are thought to pin down dislocations and prevent movement; the result is more stress required for dislocation movement. Li theory is also similar to Hall-Petch, but is based on the assumption that dislocations pile up at the grain boundaries and further prevent dislocation motion. Equations for all three theories are similar in that grain size is a major contributing factor in the stress needed to move dislocations. Equations (1) – (3) show this relationship where τ_a is resolved shear stress on the slip plane, τ_o is friction stress needed to move dislocations with no obstacles, τ_c is critical stress required to overcome grain boundary obstacles, *k* is the Hall-Petch slope, *r* is the distance from a Frank-Read source to the grain boundary, *b* is the burgers vector, and G is shear modulus. All three equations are in Hall-Petch form [10].

Hall-Petch $$\tau_a \geq \tau_o + kD^{-1/2} \quad (1)$$

Cottrell $$\tau_a = \tau_o + 2\tau_c r^{1/2} D^{-1/2} \quad (2)$$

Li $$\tau = \tau_o + GbD^{-1/2} \quad (3)$$

These equations all show that a reduction in grain diameter is inversely proportional to resolved shear stress, or more simply yield stress.

3. MMC Material Properties

Prediction of strength of a composite reinforced material is quite complex. The rule of mixtures will not apply to composite strength because strength is a structure-sensitive property (unlike elastic modulus) [10]. Composites will experience the contributions from both the matrix and reinforcement mechanical properties, or synergism, while in a composite state. Additionally, strength is affected in a composite during fabrication where the reinforcement fiber structure may be altered and fabrication temperatures can result in thermal stresses. However, several reports of CNT reinforced composite yield strength have been published. Bakshi *et al.* reported a sevenfold increase in compressive yield strength of CNT reinforced MMCs, and a tensile strength of Al-CNT composite of 194 MPa (twice that of pure Al) [5]. Kuzumaki *et al.* estimated compressive yield strength of 270 MPa for Al- 10 vol.% CNT composite using the Kelly-Tyson formula; actual results were less than the estimate due to a non-homogeneous dispersion of CNTs in the MM [11]. George et al. reported experimental yield strength of 99 MPa and ultimate tensile strength of 138 MPa for an Al- 2 vol. % CNT composite [12]. Finally, Kwon *et al.* compared true stress/strain curves of Al- 5 vol. % CNT composite to that of pure Al, the composite had a curve of more than double that of the pure Al [13]. These results all show significant improvement in strength for a CNT reinforced Al composite.

Young's modulus can be calculated for particle-reinforced composite using the rule of mixtures equation; Equation (4). Table 1 is the increase in Young's Modulus for an Al-CNT composite of 5 and 10% volume fraction of CNT.

$$E_{composite} = V_f * E_{CNT} + \left(1 - V_f\right) * E_{aluminum} \quad (4)$$

Young's Modulus (E)		
V_f	$E_{composite}$ [Gpa]	% Increase Over Aluminum
0.05	111.50	59.29
0.10	153.00	118.57

Table 1. Estimated Al-CNT MMC Young's Modulus for varying volume fraction of CNT

Thermal conductivity of CNT reinforced composites has been studied using the Eshelby equivalent inclusion model [14]. A copper (Cu) matrix reinforced with multi-walled CNT (MWCNT) was shown to have an increase in thermal conductivity from 348 W/m-K to 357.2 W/m-K with only a 1.5% volume addition of CNTs to the Cu matrix [14]. Although this study was for Cu based composites, improvement of thermal conductivity for Al is also expected [14].

The same rule of mixture analysis can be applied to the density of an Al-CNT composite. Assuming a value of 2.1 g/cm^3 for density of a CNT, a slightly negative change in the density is noted in Table 2 as increasing values for the volume fraction of CNTs added to the Al matrix.

Density		
V_f	Density [g/cm^3]	% Change Over Al
0.05	2.67	-1.11
0.10	2.64	-2.22

Table 2. Estimated Al-CNT MMC change in density for varying volume fraction of CNT

These four analyses all show the potential for a lightweight and strong composite material. The addition of a relatively small volume fraction of reinforcement can create a considerable change in the material properties of a composite. These results can be further improved by grain size reduction of the MM during processing. There are various methods of processing and consolidating MMCs. Methods used in consolidation are very important as high temperatures can create growth of the grains that were reduced in processing.

4. Consolidation Methods

Various milling methods exist for the reduction of grain size in metal powders. However, these metal powders must then be consolidated in a process that will permit the composite to be used in an armor or coating application. Achieving a high bulk density of the composite is desired in the process. Nanocrystalline materials have unique properties due to their grain size; when forming bulk material the nanostructure must be retained. Inert-gas condensation is one method that has been used, but unfortunately this method causes rapid coarsening of the nano-scale grains, even at room temperature [15]. Additionally, High Velocity Oxygen Fuel (HVOF) spray has been used for consolidation of nano-scale powders, but it is more suited for ceramics as the high temperatures will cause some amount of melting and damage to the CNTs from chemical reactions during the process [16]. Consolidating nanoparticle reinforced powders without grain growth is necessary to maintain material properties [17]. Sintering, Hot Pressing (HP) and Cold Spray (CS) are methods of consolidation that retain the nano-scale grain size of metal powders [13], [18], [19]. Of key importance in consolidation selection is keeping the temperature of the process low enough to retain the nano-scale crystal structure of the metal matrix and thus prevent damage to the CNTs [18].

a. Sintering

Sintering is a method of consolidation in which a metal powder is placed in a mold and heated to a temperature sufficient for diffusion among the atoms. Al-CNT composites have been successfully sintered with density reaching 96.1% [13]. The high density of 96.1% was reached due to reduced atmosphere exposure in a carbon mold. However, this method is not preferred as oxides on the Al surface can prevent direct contact between particles. Temperatures were also relatively close to the melting point of the Al in this process [13]. This process is effective at densification of composite powders, however due to the high temperature to achieve that density it is undesirable as a consolidation method to maintain nano-scale grain sizes and integrity of carbon nanoparticles. Additionally, the sintering process is limited in that only certain shapes of

sintered material can be made; sintered powders are restricted to the shape and size of the mold used for sintering, typically small round discs.

b. Hot Pressing

Hot Pressing (HP) is a method in which heat and pressure are applied to a metal powder at levels sufficient to sinter the material. The powders are placed in a graphite or steel mold and inductive current applied to generate heat within. Concurrent with heat application, pressure is induced through cylinders on either side of the mold. This method is common for the production of ceramic and some metallic materials. Although HP can densify nano-scale powders to full density with little grain growth, it suffers the same shortcomings as sintering in that it is limited to the size and shape of the press used [19].

c. Cold Spray Synthesis

Cold Spray (CS) is a method of consolidation that is attractive for coating or repair applications and applications that may be sensitive to high temperatures or oxidation, such as Al based coatings. CS has been compared to explosive bonding in which the particles "splat" on the surface of the substrate. Many factors affect the bonding strength of the particle splat such as velocity, temperature, and distance from the surface. Figure 2 is a CS copper on copper micrograph.

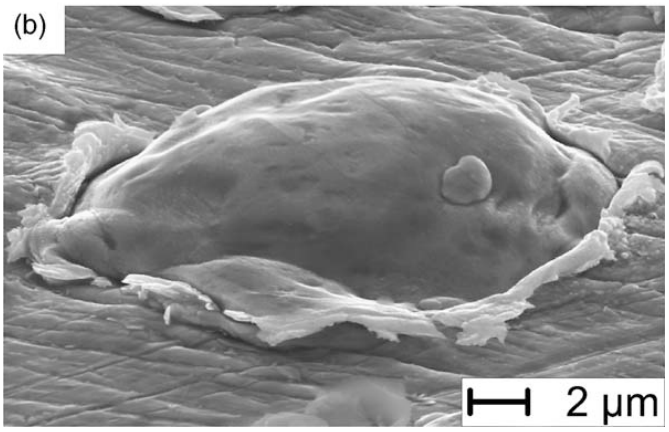

Figure 1. Scanning electron micrograph of copper particles on copper substrate from Assadi *et al.* [20]

CS uses a compressed gas (or even air) to accelerate powder particles to very high velocities. A portion of the gas used in the process is diverted through a heater, which increases the velocity as heat is transferred to kinetic energy in a supersonic nozzle. The particle-gas mixtures are sprayed through a control gun onto a suitable substrate. The kinetic energy of the particles causes strong bonding with the substrate, requiring much lower temperatures than other consolidation methods. Figure 2 is a schematic diagram of a simplified CS unit.

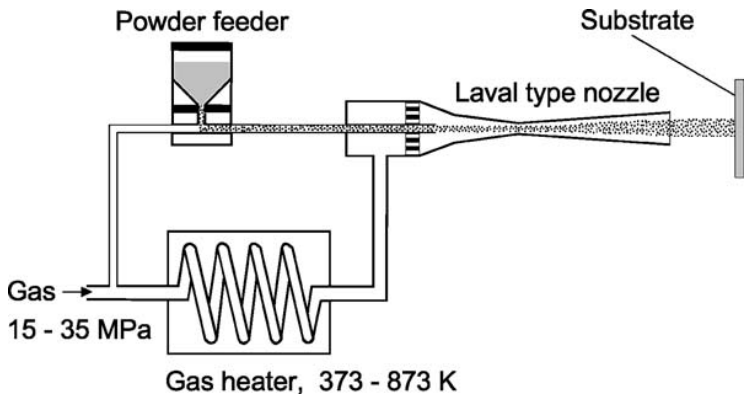

Figure 2. Schematic diagram of CS setup from Assadi *et al.* [20]

The application for CS extends well beyond that of sintering or HP as the latter are somewhat limited as to size and shape of the molds and the portability of equipment. CS has a much smaller footprint and portable units are currently available commercially. CS applications range from corrosion protection coatings, to repair of damaged parts (such as repairing ground out cracks in engine or gear casings).

Some research has been conducted using CS for CNT reinforced Al powders. S. R. Bakshi et al. successfully used CS to make 500 μm thick coatings on AA6061 substrates. A nominal composition of 0.5 and 1 weight percent CNTs were retained in the splat interfaces and embedded in the matrix. The resulting elastic modulus obtained through nanoindentation for these tests was between 191 and 229 GPa for the CNT reinforced Al coatings [18].

C. MECHANICAL ALLOYING TECHNIQUES

1. Synopsis

Mechanical Alloying (MA) is powder processing technique that is used to produce materials from a blend of elemental powders through repeated welding, fracture, and rewelding [21]. Through MA, powders can be processed to reduce grain size and/or mix different materials to produce a homogenous mixed powder. There are several MA techniques, but the most common is high-energy ball milling. Milling refers to an additional process used to refine powders to a uniform configuration. MA was first developed to produce Oxide-Dispersion Strengthened (ODS) nickel and iron based superalloys. More recently, MA has been shown to effectively produce a variety of MMC alloys [21].

The basic principle of MA is that kinetic energy from the milling media (steel or ceramic balls, or impactors) is forced onto the sample powder, pulverizing it into smaller particles. When the milling media interacts with the sample the force causes the sample to fracture. Cold welding of the sample is common, and specific materials may be added to the mixture to minimize cold welding and agglomeration. These are known as process control agents (PCA). PCAs such as stearic acid in small quantities have been shown to effectively reduce agglomeration of powders that are MA [21].

2. Types of Mechanical Alloying

a. High Energy Ball Mill

A high-energy ball mill is one that uses a hardened vial, typically steel, and ball milling media, either steel or ceramic, to MA a sample. SPEX shaker mills are commonly used in MA. The SPEX shaker mill vibrates a sample in a figure eight pattern with amplitude of about five cm and speed of 1200 rpm. The shaking created by the machine causes the milling balls to impart kinetic energy onto the sample. The velocity of the media is near 5 m/s, creating high amounts of energy for impacting the sample [22]. Various combinations of vials and milling media can be used in a high-energy ball mill. Ball to powder ratio, or BPR, is commonly used to vary milling parameters. High-energy ball mills are somewhat limited in powder production in that only limited amounts

of powder can be used. 30 grams per vial is the typically the upper limit of high-energy ball mill capacity. Figure 3 is a representation of high-energy ball milling with powders being milled between the milling ball media and the outer wall of the vial. Milling occurs by both shearing and impact [23].

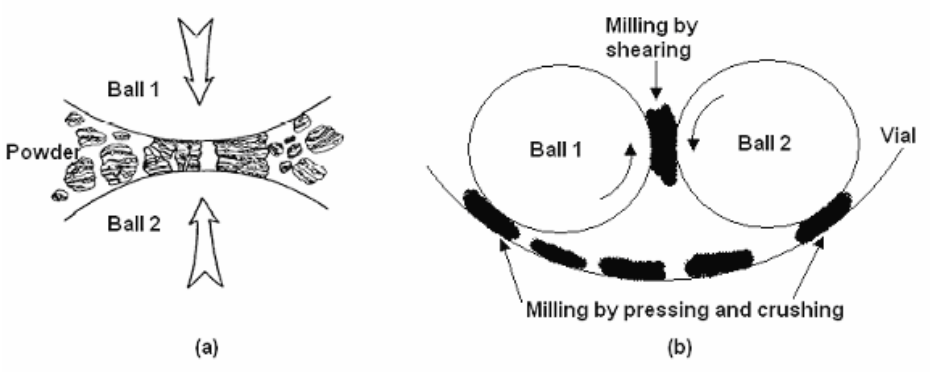

Figure 3. High energy ball milling interactions between milling balls (a), and the vial wall (b) from Calka *et al.* [23]

b. Planetary Mill

Planetary mills are also a common method for MA of powders. They differ from high-energy ball mills in that the media is not shaken. Instead the grinding vial is placed in a machine that spins it around a vertical axis. Additionally, the grinding vial itself is also rotated, but counter to the axis. This creates opposing centrifugal forces, which force the grinding media to run along the inside of the vial. This action creates friction between the vial and grinding balls. When the two centrifugal axes align, the grinding balls are forced to the other side of the vial causing an impact to the powder being milled. Figure 4 is an image of the grinding motion within a planetary ball mill.

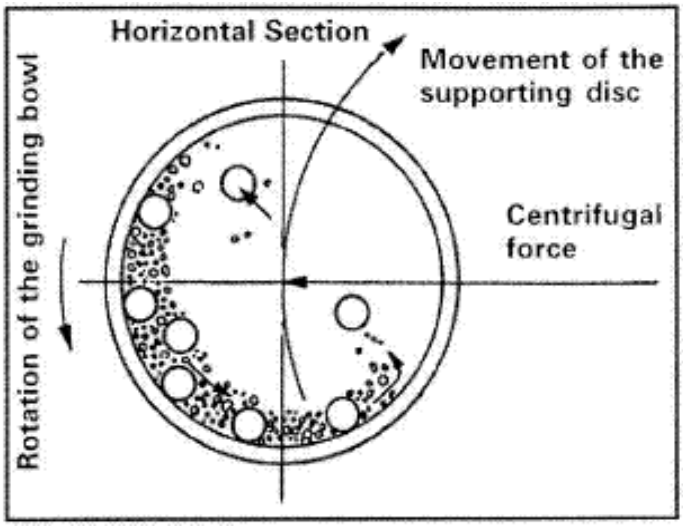

Figure 4. Planetary ball mill grinding motion from Suryanarayana [21]

c. Attritor Mill

Mechanical attritors use a drum and internal impellers to agitate grinding media and process powders. As the impellers spin within the drum, the grinding balls interact with each other, the impellers, and the drum [21]. This is a low energy method of milling as the speed of the impellers is rather slow at 250 rpm in comparison to that of high-energy ball milling or planetary mills. Mechanical attritors have the advantage of large-scale production with capacities between 0.5 and 40 kg [21]. Figure 4 is an image of a mechanical attritor internals.

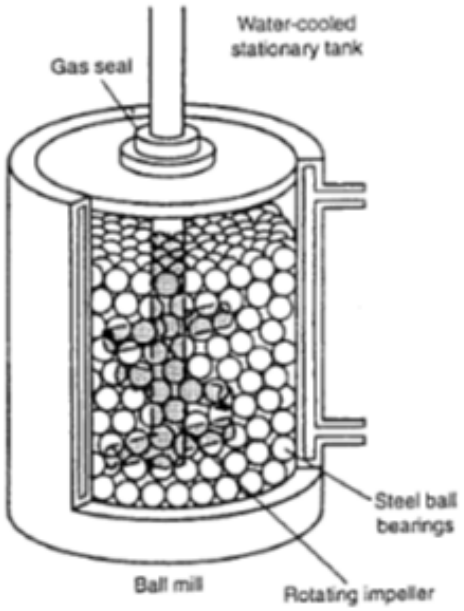

Figure 5. Mechanical attritor internals from Suryanarayana [21]

d. Cryogenic Mill

Cryogenic mills use liquid nitrogen (LN) to supercool the sample and the grinding vial. The most common cryogenic mill is the SPEX Freezer/Mill. This machine uses a magnetic coil to shake a vial and impactor submerged in liquid nitrogen. Unlike high-energy ball mills, cryogenic mills typically have only one impactor that is shaken horizontally in the mill. As the impactor collides with each end of a hardened steel vial end, the powder is pulverized. These mills require a considerable amount of resources; the LN boils off rather quickly and without an automated level control, requires frequent monitoring and refilling of the LN. Cryogenic mills have the advantage of milling in a super-cooled environment of about -200C. This very low temperature can reduce cold welding of metal materials and improve the milling time for grain size reduction.

3. MA Process Variables

Various parameters in MA will affect the resultant materials that are alloyed. The materials used for milling, amount of material in relation to the grinding media (eg. ball to powder ratio or BPR), atmosphere, amount and type of PCAs, milling time, and

temperature will all have an effect on the milling process [21]. Careful documentation of the various parameters is needed for reproducibility and confirmation of experiments. Often small samples will be made for the purpose of material characterization, with large-scale reproduction to happen at a later time.

The type of media used for milling can have an effect on the milling process. Steel, ceramic, and plastics are commonly used as grinding media. When using these materials in a high-energy environment, contamination and/or chemical reaction of the composite is of concern. The most common type of contamination found in high energy milling is due to iron contamination from the grinding media and vials, with milling time as the biggest factor in contributing to powder contamination [21]. Longer milling times will often result in powder contamination. Between one and four percent of iron contamination is common in milling procedures that use steel as a grinding media; iron contamination has also been as high as 33% in some Tungsten milling experiments [24].

The BPR is also a major contributing factor in the final product. In high-energy ball milling, this variable is called the ball to powder ratio. Typical values of this ratio range between 10:1 and 30:1 [21]. This ratio can greatly affect the finished powder, as the impact energies are different for different ratios. Some data has shown that increasing this ratio can lead to particle growth [25].

Atmosphere in which the powder is milled is a concern for reactive metals such as Al. Oxide formation can be minimized by filling the grinding vials in an inert atmosphere such as Argon (Ar).

Process control agents are typically used to prevent agglomeration of the MM during alloying. PCAs act as a surfactant or lubricant and reduce the cold welding effect during alloying. The PCA will be adsorbed on the surface of particles and interfere with cold welding by lowering the surface tension [21]. Stearic acid is commonly used in three percent or less when alloying Al samples.

D. THESIS OBJECTIVES

This research is being conducted in the scope of a larger NPS research effort that aims to design a new class of lightweight, nanocarbon-reinforced metal armor via cold spray synthesis. The primary objective of this thesis is to fabricate Al-CNT composite powders using cryogenic milling.

This study will investigate the feasibility of CNT reinforced A1. Al-CNT MMCs may allow for the development of new, lightweight armor materials with improvements in fragment resistance, as compared to conventional polymer-based composites. Metal processing techniques that use high temperatures and pressures are not suitable for Al-CNT synthesis as the CNTs are damaged and/or chemically react with the metal matrix, thus degrading the mechanical properties of the composite. These challenges can be overcome by using cryogenic MA followed by consolidation via CS.

In order to obtain a composite with isotropic properties, CNTs must be well dispersed within the Al matrix. Cryogenic milling provides a method to disperse the CNT in the metal powder prior to cold spray, while preventing excessive particle agglomeration and cold-welding of Al.

In particular, the following tasks will be performed:

- Synthesize Al-CNT composite powders via cryogenic milling and determine feasibility of for MMC fabrication
- Investigate effect of milling parameters such as cycle time, cycle number and CNT content on the structural and mechanical characteristics of the composite powder
- Determine changes in crystal size, particle size, and particle shape upon milling
- Study the effect of milling on the structural integrity of the CNTs
- Homogeneously disperse CNTs in the MMC
- Produce nanometer scale (<100 nm) crystallite or grain sizes.

II. EXPERIMENTAL PROCEDURE

A. MATERIALS

Aluminum was processed with MWCNTs and stearic acid as a PCA in this study. Ar was used to maintain an inert atmosphere during processing in a liquid nitrogen (LN) filled mill. Table 3 lists the materials used for this study.

Micro-Scale Aluminum Powder
Spray Atomized Aluminum Powder (Valimet)
spherical particles
average size: 15 μm
325 mesh
99.7% purity

Carbon Nanotubes
MWCNT (Arkema Graphistrength)
number of walls: 5-15
average diameter: 10-15 nm
length: 0.1-10 μm
> 90 to 97% purity

Process Control Agent
Stearic Acid (Sigma-Aldrich)
Face Centered Cubic (FCC)
> 95% Purity

Table 3. Materials used for research

B. COMPOSITE SYNTHESIS

The machine used to MA the micro-Al powder with MWCNTs and stearic acid was a SPEX SamplePrep 6870 Freezer/Mill. The mill is filled with LN and a vial/impactor set is placed in a shaker driven by a magnetic coil to pulverize the powder mixture. The 6870 Freezer/Mill has various user controls for selection of milling parameters. When run, there is a pre-cool cycle that runs before the milling cycle begins. The pre-cool cycle is adjustable between one and 20 minutes. The frequency of the shaker is also adjustable between 10 and 15 cycles per second. Milling is completed in a

number of cycles ranging between one and 15, with each cycle having a run time between one and 10 minutes. Cooling time between cycles is also adjustable. The following parameters were kept constant for all experiments:

Pre-cool time: 10 minutes (default setting)

Frequency: 12 cycles per second

Cooling time between cycles: 2 minutes (default setting)

These parameters were selected to keep most parameters constant while varying the cycle number and cycle times. Additionally, the use of LN in the Freezer/Mill requires near constant monitoring. LN boils off rather quickly; selection of extended pre-cool times or cooling times between cycles would require addition of LN during some of the longer run experiments. This was not an acceptable option without the use of an automated LN level control system that must be installed by SPEX. Figure 7 is an inside image of the mill. The shaker assembly is lowered in the LN filled tub.

Figure 6. SPEX 6870 SamplePrep 6870 Freezer/Mill used to mechanically alloy AL-CNT powders

The vials used in the mill were the SPEX 6751 small grinding vial set. The vial itself is clear plastic tube to which hardened steel ends are attached along with a hardened

steel impactor within. The small vials have a capacity of 0.5 to 4 grams. Figure 8 is the small vial/impactor set used for all milling experiments.

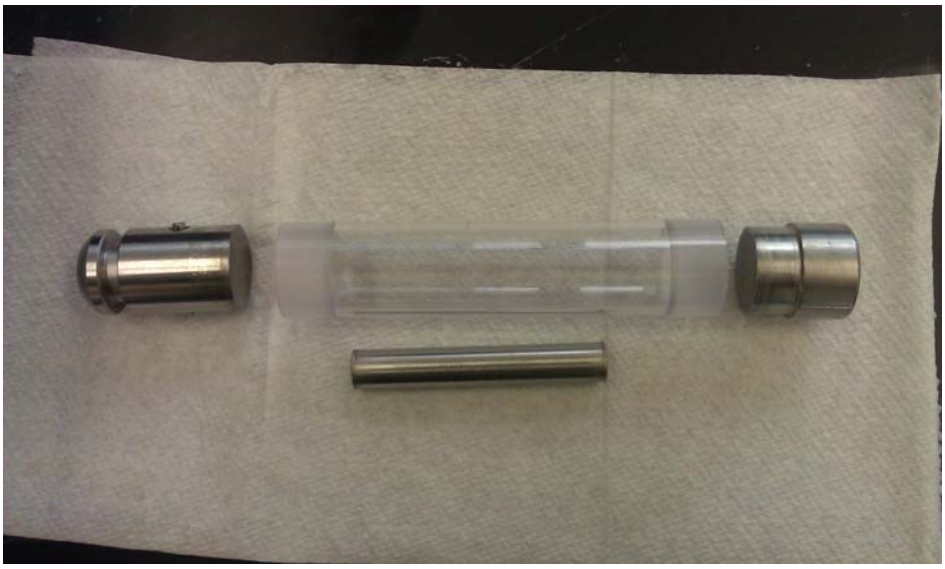

Figure 7. SPEX small grinding vial and impactor

In addition to the equipment used to for milling, all materials were weighed using a Denver Instruments Precision Lab Scale and assembled in a controlled atmosphere environment. To ensure an inert atmosphere and prevent oxidation of the Al powder during milling, the weighed Al powder, MWCNTs, and stearic acid were all placed in Ar. The small grinding vial was filled with the materials and impactor with only the bottom end of the vial assembled. The vial was then placed in an Ar filled glove box and top end of the vial assembled. This process ensured the vial and powders were only exposed to Ar for milling. Figure 8 is an image of the glove box used for vial assembly in Ar.

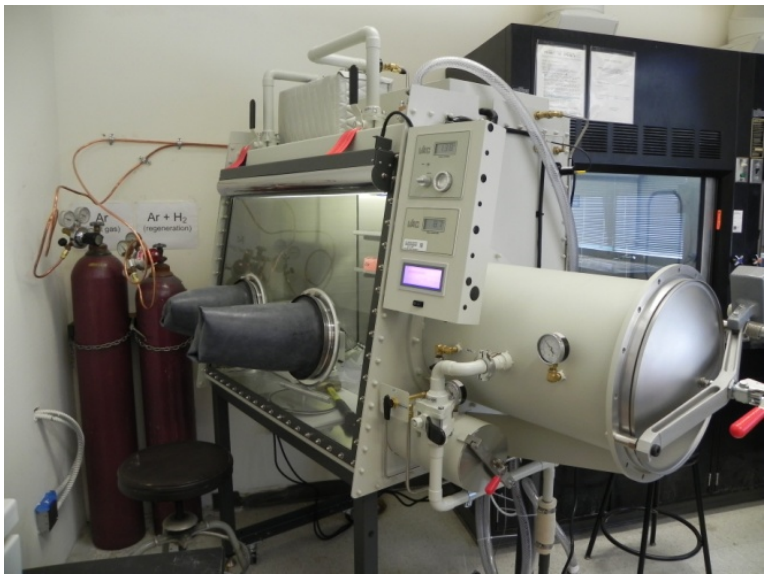

Figure 8. Vacuum Atmosphere Control, Inc. glove box.

To determine the basic settings and operation of the 6870 Freezer/Mill using Al, three simplified experiments were run using Al flakes. Al flake that was used is 1mm, 99.99% purity by trace metals basis (Sigma-Aldrich, Inc., St. Louis, MO). The first of the experiments was to mill the 1.5 grams of flake for three cycles of five minutes each. The second and third experiments also used 1.5 grams of Al flake, but included the use of 3%, by weight, of stearic acid. The second experiment was milled for another three cycles of five minutes each, and the third for six cycles of 10 minutes each. Other milling parameters were maintained constant as previously noted.

The result from the first experiment was severe agglomeration of the Al flake. The following two samples showed a significant reduction in agglomeration of the Al, as well as a visually noticeable reduction of particle size. In the sample that was milled for a total of 60 minutes, the result was mostly Al powder with few large size visible particles indicating a large distribution of particle size. These Al powders are shown in Figure 9.

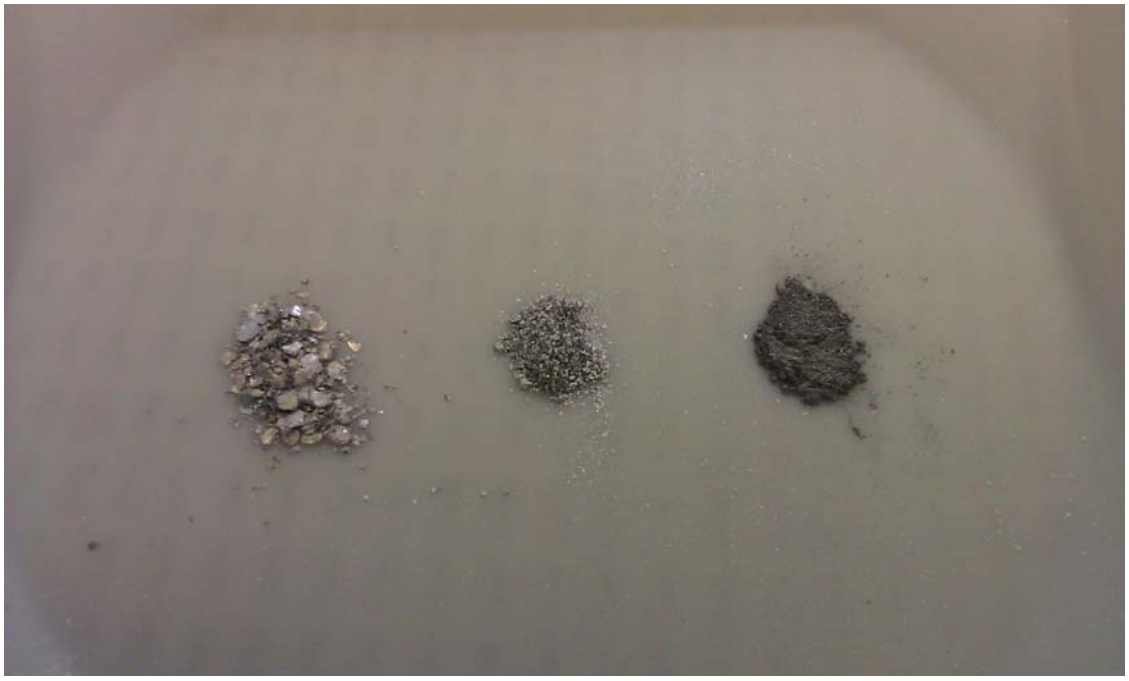

Figure 9. Cryo-milled Al flake for 15 min without PCA; 15 and 60 minutes with stearic acid PCA (from left to right)

For all remaining experiments, 3% by weight stearic acid was used as the stearic acid PCA addition significantly reduced agglomeration of the Al based powders and sticking to the hardened metal impactor and ends.

From the three experiments with Al flake and with information contained in similar studies and literature, a matrix of 27 experiments using micro Al powder and MWCNTs was developed. This matrix varies the cycle and run times of the Freezer/Mill for various weight additions of MWCNTs. Table 4 shows the experiments conducted for this study.

Experiment	CNT Weight Concentration	Run Time [1-10 min]	Number of Cycles [1-15]	Mass $_{Al}$ [g]	Mass $_{CNT}$ [g]	Mass $_{SA}$ [g]
AlCNT-1-1	0%	2	3	1.5	0	0.045
AlCNT-1-2	0%	2	6			
AlCNT-1-3	0%	2	9			
AlCNT-1-4	0%	5	3	1.5	0	0.045
AlCNT-1-5	0%	5	6			
AlCNT-1-6	0%	5	9			
AlCNT-1-7	0%	10	3	1.5	0	0.045
AlCNT-1-8	0%	10	6			
AlCNT-1-9	0%	10	9			
AlCNT-2-1	5%	2	3	1.5	0.075	0.045
AlCNT-2-2	5%	2	6			
AlCNT-2-3	5%	2	9			
AlCNT-2-4	5%	5	3	1.5	0.075	0.045
AlCNT-2-5	5%	5	6			
AlCNT-2-6	5%	5	9			
AlCNT-2-7	5%	10	3	1.5	0.075	0.045
AlCNT-2-8	5%	10	6			
AlCNT-2-9	5%	10	9			
AlCNT-3-1	10%	2	3	1.5	0.15	0.045
AlCNT-3-2	10%	2	6			
AlCNT-3-3	10%	2	9			
AlCNT-3-4	10%	5	3	1.5	0.15	0.045
AlCNT-3-5	10%	5	6			
AlCNT-3-6	10%	5	9			
AlCNT-3-7	10%	10	3	1.5	0.15	0.045
AlCNT-3-8	10%	10	6			
AlCNT-3-9	10%	10	9			

Table 4. Experiment matrix with varied milling cycle and run times

Samples were milled for various times and cycles ranging between six and 90 minutes of total milling time. Experiments were not conducted beyond a 90-minute maximum milling time due to LN boiling off during operation. Based on the level in the tub after 60 minutes with a 10 minute precool cycle in the preliminary experiments, it was determined that approximately 90 minutes was the maximum mill time without need to refill LN during operation.

The purpose of the 27 experiments is to characterize the MMCs for use in CS. There are some properties of the MMCs that are required, these are:

- Homogeneous dispersion of the CNTs in the MMC
- Particle size of approximately 60 μm
- Nanometer scale (<100 nm) crystallite or grain size

Homogenous dispersion is necessary for the uniform material properties of the coating applied with CS. Particle size of the MMC is important as the particles need to be large enough that they can accelerated and have kinetic energy from CS synthesis. For CS synthesis to be successful, Al particles must be accelerated over 700 m/s [26]. Work on similarly cryogenically milled Al powders has shown that particles with a size of 58 μm can be accelerated to this speed [26]. The nanometer scale is defined as <100 nm. Achieving small grain, or crystallite, sizes is highly desired for these experiments as the purpose is to achieve higher strength with grain size reduction. It has been shown that through the MA process, that a powder can exhibit very small grain size; between 2 and 5 nm [27].

As the experiments were completed, the vial was immediately placed in a plastic bag to prevent condensation on the surface of the vial. When the vial returned to room temperature the contents were removed using an extractor from SPEX and placed in labeled glass vials for characterization.

C. MATERIAL CHARACTERIZATION

1. X-Ray Diffraction

X-ray diffraction (XRD) is a crystallography characterization method used where x-rays are aimed in a beam at a sample. As the beam strikes the crystal planes of the sample, scattered beams are picked up by a sensor to create a diffraction pattern. As the sample is rotated through various angles, the strength of the diffraction pattern as well as the angle are recorded. These angles are known as the 2θ angles and range between 0 and 170 degrees. Plotting the strength, or intensity, versus the diffraction angle will yield peaks at certain angles depending on the material being analyzed.

For this study the equipment and settings used for X-ray diffraction is listed in Table 5.

XRD Equipment and Settings
Phillips PW 1830 Diffractometer
2θ diffraction angles between 20 and 120 degrees
Accelerating voltage: 35 kV
Anode current: 30mA
Copper anode x-ray radiation energy: 8.04 keV
Copper anode x-ray wavelength: 0.154 nm

Table 5. XRD equipment and settings

The 2θ used result in intensities for eight peaks of Al. The higher angle peaks are typically wider and yield less useful data due to the nature of diffraction at high angles. A zero background powder holder from VDL Enabling Technologies Group held all samples. The sample holder is made from silica that is cut on a plane such that there are no Bragg angle peaks; this eliminates background radiation during the analysis typically seen when sample powders are secured to a glass slide using silicone grease. The sample holder is unique in that it has a small concave area to hold powders. Figure 10 is the zero background sample holder.

Figure 10. Zero background XRD sample holder

XRD data for analysis in this study was collected using X'Pert Data Collector software. The data was then analyzed using X'Pert HighScore software. The HighScore

software was set up with a shape factor of 0.6 and wavelength of 0.154 nm. The shape factor is the percentage Lorentzian to Gaussian used by the software in profile fitting. When the raw data is opened in the software, a series of steps to remove the k-alpha2 peaks was performed. First, the background is determined followed by a profile fit by the software. This profile fit will produce a first-pass Pseudo-Voigt (P-V) curve fit of peaks and put results in a tabular list. Selecting each individual peak and using the fit data function further fits the peak list and adds all k-alpha2 peaks to the list. While this is done an R^2 calculation is simultaneously performed by the software that yields an error value for the process. R^2 values for the 27 experiments were typically below 5%. After all peaks are identified in the peak list, the k-alpha2 peaks are stripped yielding only the Al peaks. The full width half maximum (FWHM) and 2θ angles are included with the Al peak data. This data was exported in .csv format to Microsoft Excel for further analysis of grain size and microstrain using Williamson-Hall (W-H) analysis.

Plotting intensity vs. 2θ values shows a peak for the material being analyzed at that particular angle. Peak broadening is a result that occurs when grain size is reduced. When multiple plots are overlaid on each other the resulting peak broadening can be seen. Figure 8 is an example of peak broadening for identical samples in which cryo-milling time was increased. The data used in Figure 11 is raw data before k-alpha2 peaks were removed; the k-alpha2 peak is clearly visible in the As-Received Al powder curve.

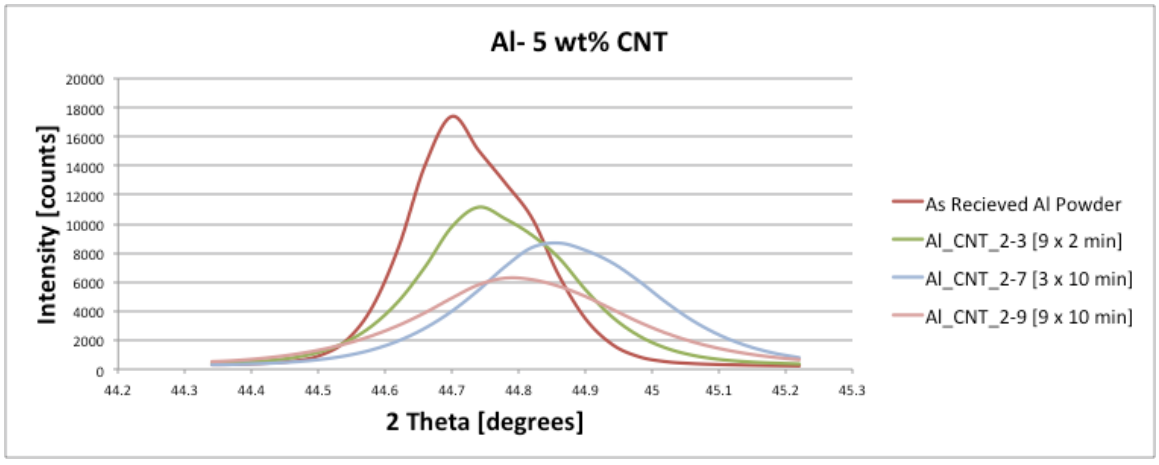

Figure 11. Peak broadening from reduction of grain size

The integral width, or breadth, of diffraction peaks in nanocrystalline materials is a function of crystallite size and microstrain. The W-H analysis is a method of calculating both the crystallite size and microstrain by using a form of the Scherrer and Wilson-Stokes equations. However, the XRD instrument also broadens the peak width, which adds error to the W-H analysis. To overcome this error and subtract it out in the W-H analysis the peak broadening from the instrument must be found. Instrument broadening was found by XRD analysis of a strain free powder. Lanthanum Hexaboride, sample 660b, from the National Institute of Standards and Technology (NIST) was analyzed using the same XRD equipment. The data used for instrument broadening was collected by LT Brian Sneed [6]. Taking the FWHM of the 660b sample and plotting it against the 2θ value will provide a curve showing the instrument broadening effect over the full range of angles used for analysis of Al-CNT composite powders. Figure 12 displays the instrument broadening data plot for the XRD equipment used in this study.

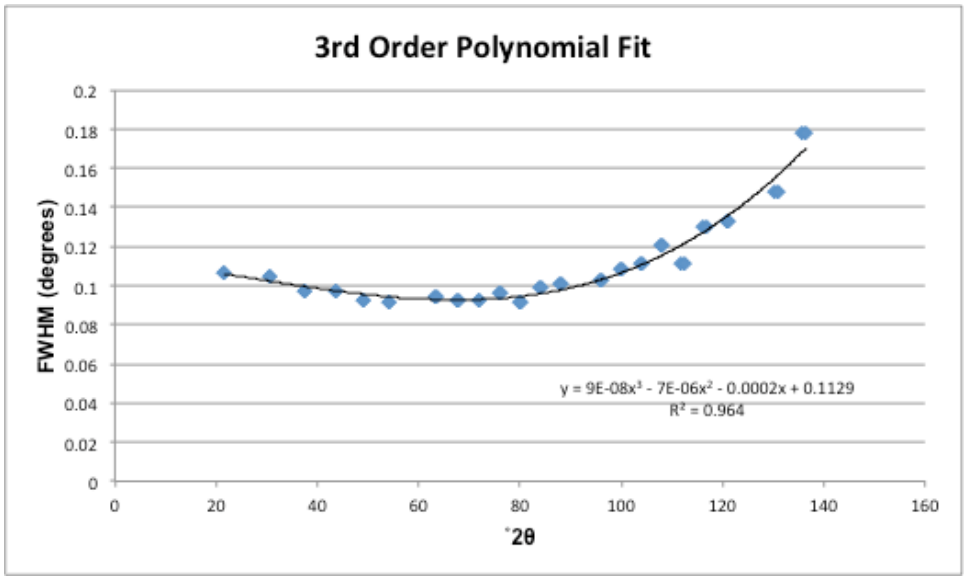

Figure 12. NIST standard 660b , FWHM plotted over 2θ angles between 20 and 140 degrees

A third order polynomial was fit to the curve date and an equation for the curve generated using a trend line in Microsoft Excel. The equation of this curve was then plotted through the same values of 2θ angles as a check of the curve fitment. Figure 13 is this curve.

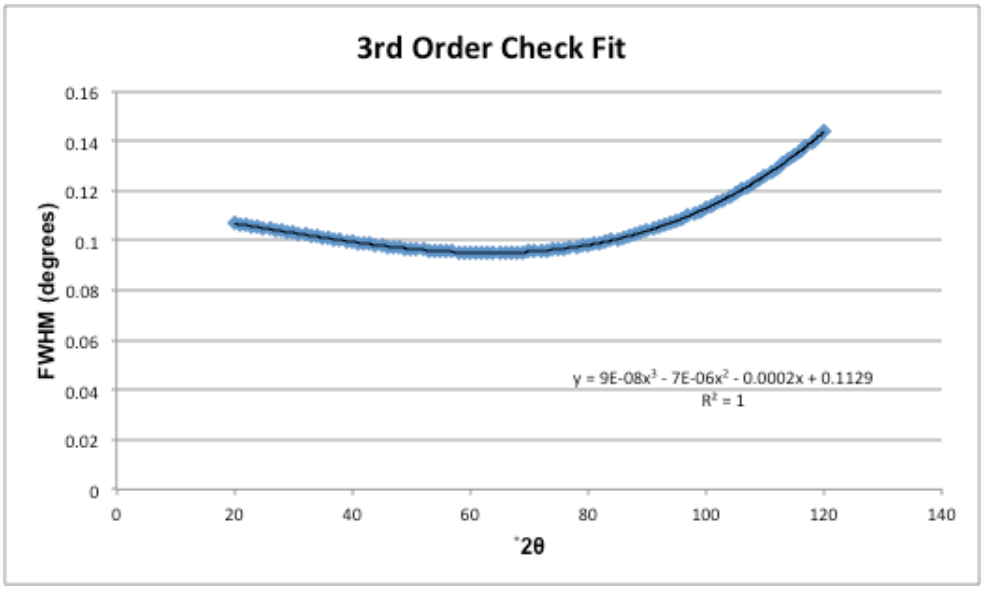

Figure 13. Equation used for instrument broadening 2θ angles between 20 and 140 degrees

2. Nanoindentation

The second method of characterization of Al-CNT powders in this study was conducted by nanoindentation. Nanoindentation is a method for hardness testing of small samples. For this study an Agilent Technologies G200 Nano indenter was used. The indenter is based on an electromagnetic transducer with a diamond indentation tip. The machine is vibration isolated and enclosed under a hood during operation. The objectives used were both 10x and 100x; 10x primarily for focusing the instrument and 100x for locating and selecting sample indentation sites. The indenter itself is forced via the electromagnetic transducer and corresponding displacement collected via a capacitance gauge. Data collected during indentation such as load, displacement, and stiffness are

recorded and further used to calculate elastic modulus using the Oliver-Pharr (O-P) method [22]. The elastic modulus is found from Equation (5) and hardness from Equation (6).

$$E = \frac{\sqrt{\pi}}{2} * \frac{S}{\sqrt{A}} \tag{5}$$

$$H = \frac{P_{\max}}{A} \tag{6}$$

Where E is the elastic modulus, S is stiffness, A is the projected area of contact [23], H is hardness, and P_{max} is the maximum indentation load.

All nanoindentation tests were conducted using the G-Series CSM Standard Hardness, Modulus, and Tip Cal indentation method. This testing method records both elastic modulus and hardness for each analysis point as a function of depth. All samples were conducted with the settings shown in Table 6 using Nanosuite software.

Nanosuite Software/Nanoindenter Settings
Berkovich tip serial number: TB15658
x-spacing: 5 µm
y-spacing: 5 µm
Surface approach distance: 1000 nm
Surface approach speed: 10 nm/sec
Surface detect stiffness criteria: 200 N/m
Poisson's ratio: 0.3
Maximam drift rate: 0.04 nm/s
Strain rate target: 0.05 s-1
CSM harmonic displacement: 2nm
CSM harmonic frequency: 45 Hz
Maximum drift delay time: 5 hrs

Table 6. Nanoindentation settings

The indenter was calibrated for each batch run using the software calibration tool on a fused silica calibration specimen. Ten indentation locations were manually identified on individual powder particles for each sample using the 100x objective and data recorded.

Sample preparation for nanoindentation used a two-part epoxy. Struers EpoFix epoxy was used for all samples. A small sample of Al-CNT powder, approximately 0.25 grams was mixed with a very small amount of prepared epoxy. Typically, four or five drops of the epoxy would be sufficient to mix with a powder and form dense paste. This mixture was carefully transferred to the bottom of silicone oil lined mold. Once the powder sample was placed in the mold, the remaining epoxy was poured in over the powder mixture to a thickness of approximately 1 cm. After curing the epoxy pucks were polished by first leveling with 800 grit paper, and then followed by manual felt polishing using solutions of both 0.1 and 0.05 μm aluminum oxide. Polishing was conducted in steps of approximately 10 minutes each using each of the two aluminum oxide solutions on separate felt pads under running water. Care was taken during felt polishing to only use light pressure by hand as the EpoFix epoxy had a tendency to smear at porous locations on the puck. Following polishing, the pucks were mounted on steel mounts for use in the nanoindenter stage. Figure 14 is an image of a prepared sample puck prior to polishing.

Figure 14. EpoFix epoxy mounted Al-CNT powder sample

Aglilent Nanosuite software was also used to collect images of the epoxy-mounted samples using the add-on program MSnap3. Images were taken using both a 10x and 100x objective with a legend of 10 μm over several sites in the samples. This

was useful in showing the plastic deformation and shearing of the particles due to cryo-milling and the characteristics of individual particles.

3. Particle Size Analysis

A Horiba Partica LA-950 laser diffraction particle size analyzer was used for particle size analysis of select Al-CNT powders. Between 200 and 400 mg of each powder was added to a chamber filled with pure isopropanol to suspend the powders in solution. A small magnetic stirring device keeps the particles suspended while the machine is operated. This clear chamber with a suspension of particles can be seen in Figure 15.

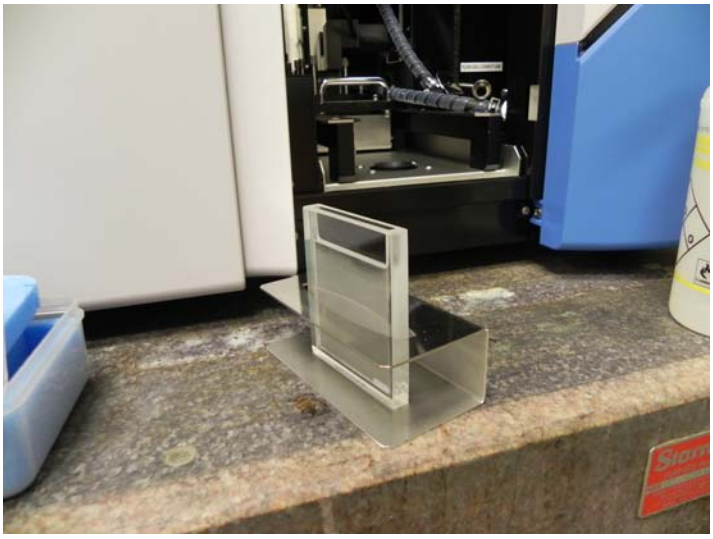

Figure 15. Suspended powder in isopropanol for laser diffraction analysis

The analyzer has a sizing range between 0.01 and 3000 μm with accuracy within 0.6%. The principal of operation of laser diffraction is that light will scatter more intensely at smaller angels for larger sized particles. Measuring this scattered light from sample particles is then used in a Mie algorithm to determine particle size [28]. The software included with the analyzer will produce a distribution and percent undersize graph for the sample.

4. Raman Spectroscopy

An inVia Confocal Raman Microspectrometer (Renishaw Inc.) was used for analysis a D and G bands for selected Al-CNT composite samples. All samples were analyzed using a 514 nm laser. Analysis of the ratios between the D and G bands provides some indication as to the structural integrity of the CNTs after milling. Samples analyzed were compared to an as-received CNT sample. Using the included software, the background can be removed and ratios of D and G band intensities calculated and compared.

THIS PAGE INTENTIONALLY LEFT BLANK

III. RESULTS AND DISCUSSION

A. PRELIMINARY EXPERIMENTS

When the sample that was milled for 60 min was exposed to air (cap removed from a small sample vial) under an evacuation hood, oxidation of the exposed Al surfaces on the particles was noticed visually. The temperature of the oxidizing sample in the vial was hot to the touch and visual indication of oxidation noticeable. This can be seen in Figure 16.

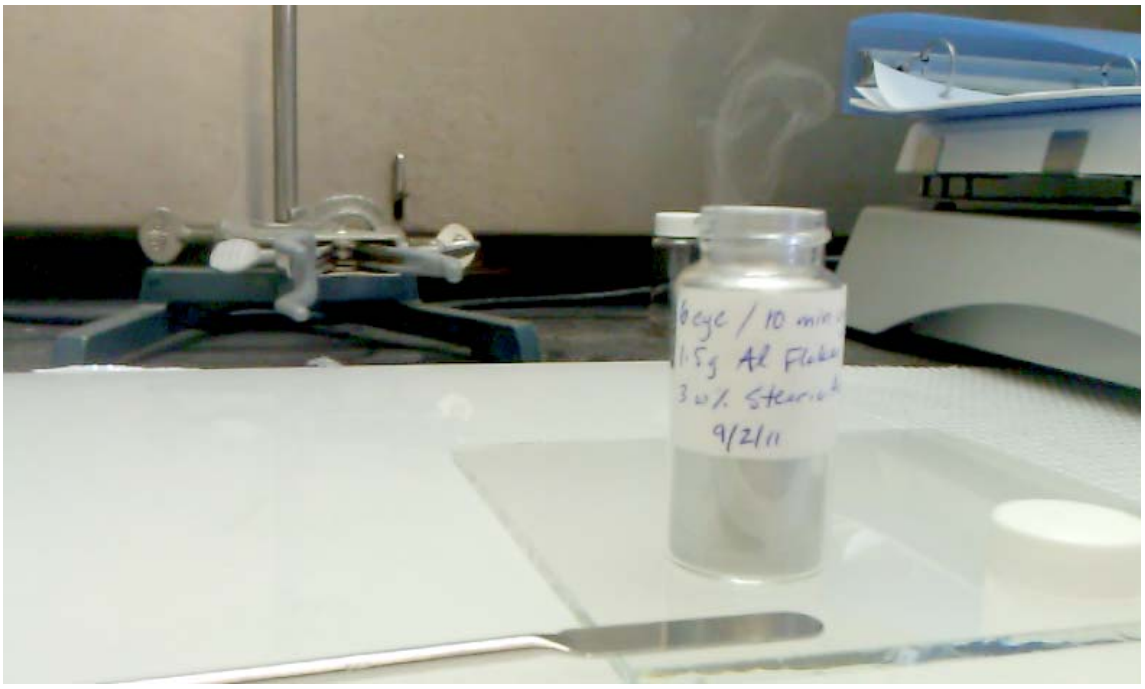

Figure 16. Al flake milled for 60 minutes total; oxidation of Al exposed to air

For the remaining 27 experiments to be conducted, samples milled over 45 min were placed in sample vials in an Ar atmosphere within a glove box to prevent the rapid oxidation observed in air.

B. POWDER MORPHOLOGY

1. As-Received Aluminum Powder

An SEM micrograph of the as received Al powder detailed in Section II is shown in Figure 17. The Al powder was spherical shaped and the analysis by both SEM and laser diffraction agree with the manufacturer's supplied data.

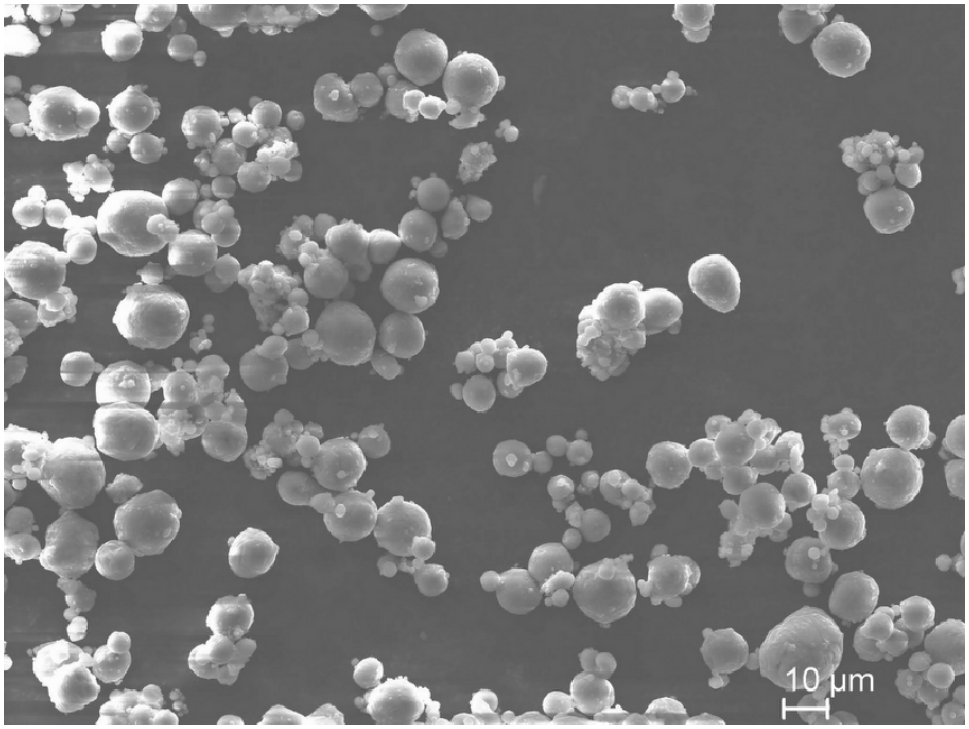

Figure 17. SEM micrograph of as received micro-aluminum powder

2. Mechanically Alloyed As-Received Aluminum Powder

As noted in Section II, a control group of experiments containing no CNTs was also milled in the SPEX Freezer/Mill. The longest milled pure Al powder was analyzed using SEM. This sample was milled for a total of 90 minutes; 9 cycles of 10 minutes (maximum setting). The characteristic shape and size of particles milled via this method are shown in Figure 18. SEM analysis was not conducted on the powders containing MWCNTs.

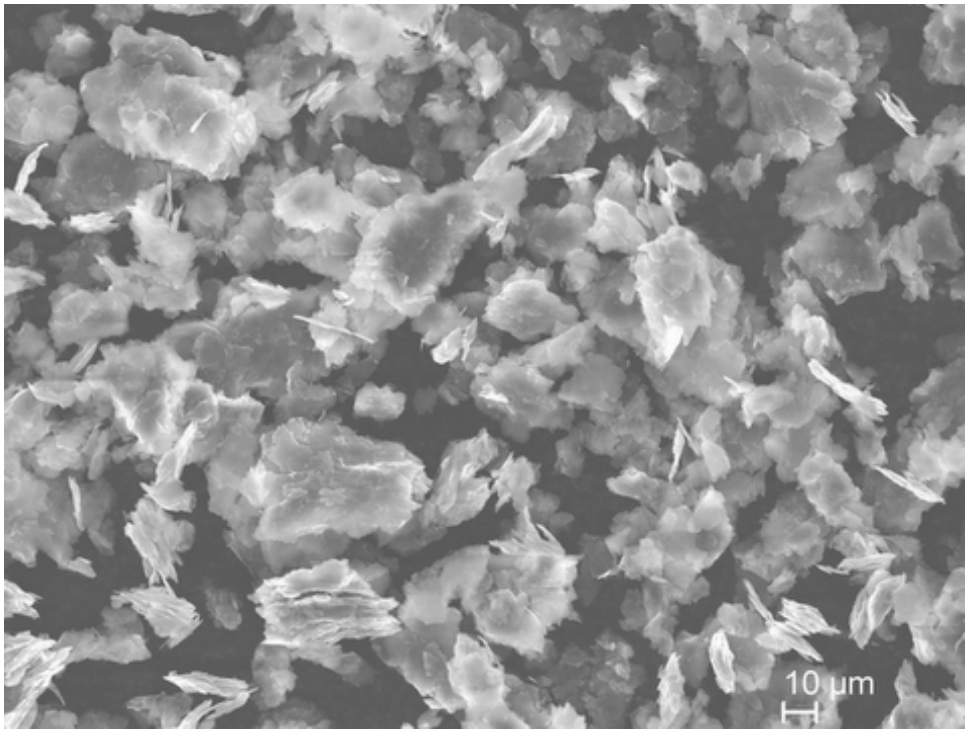

Figure 18. Micro scale Al milled for a total of 90 minutes (SEM micrograph, secondary electron image 20 keV)

3. Mechanically Alloyed Al-CNT Powders

Although SEM analysis was not conducted on the powders containing CNTs, a select number of samples were analyzed using laser refraction to determine particle size and size distribution curves of these powders. Both the shortest and longest milled powders, as well as a 60-minute total mill time and the as-received powder, were analyzed using this method. Regardless of milling time, the mean values for particle size remained fairly constant. The average size of approximately 20 microns was observed for all samples that were analyzed in the particle size analyzer. An example of distribution and percent undersize curves are shown in Figure 19.

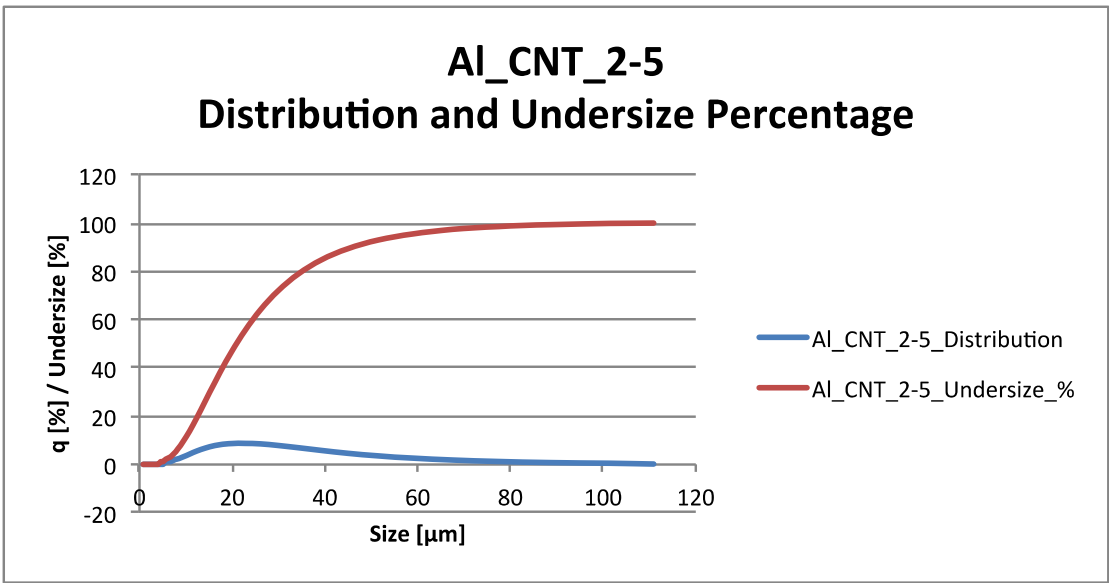

Figure 19. Distribution and undersize percentage curves for selected Al-CNT powder

The blue distribution curves from both the as-received Al powder and select 5-wt% CNT powders are combined and shown in Figure 20. Although the average particle size of approximately 20 microns remains fairly constant between samples, a broadening of the curves occurs for longer milled samples. This shows some of particle growth with a fraction of particles of about 100 microns for samples milled 30 minutes or more. Results from identical milling conditions, but with 10 weight percent CNTs were similar.

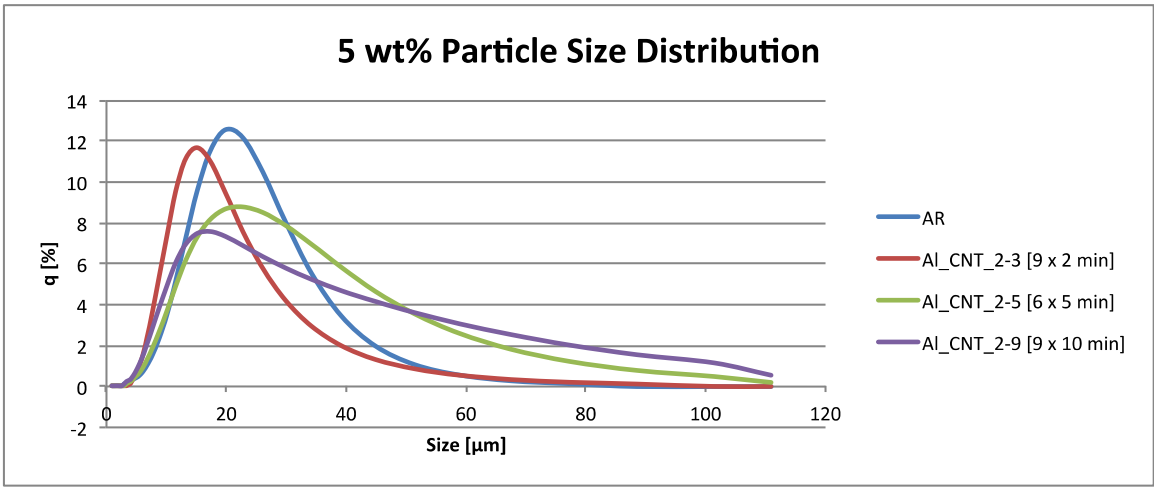

Figure 20. Size distribution curves for as-received and Al - 5 wt.% CNT powders

Optical images using 10x and 100x images were also taken of select Al-CNT powders. The powders were mounted in epoxy pucks as described in Section II. Optical analysis of these powders is consistent with the particle size analyzer data, and shows mostly platelet shaped particles. 10x and 100x images of a 5 weight percent CNT powders are shown in Figures 21 and 22.

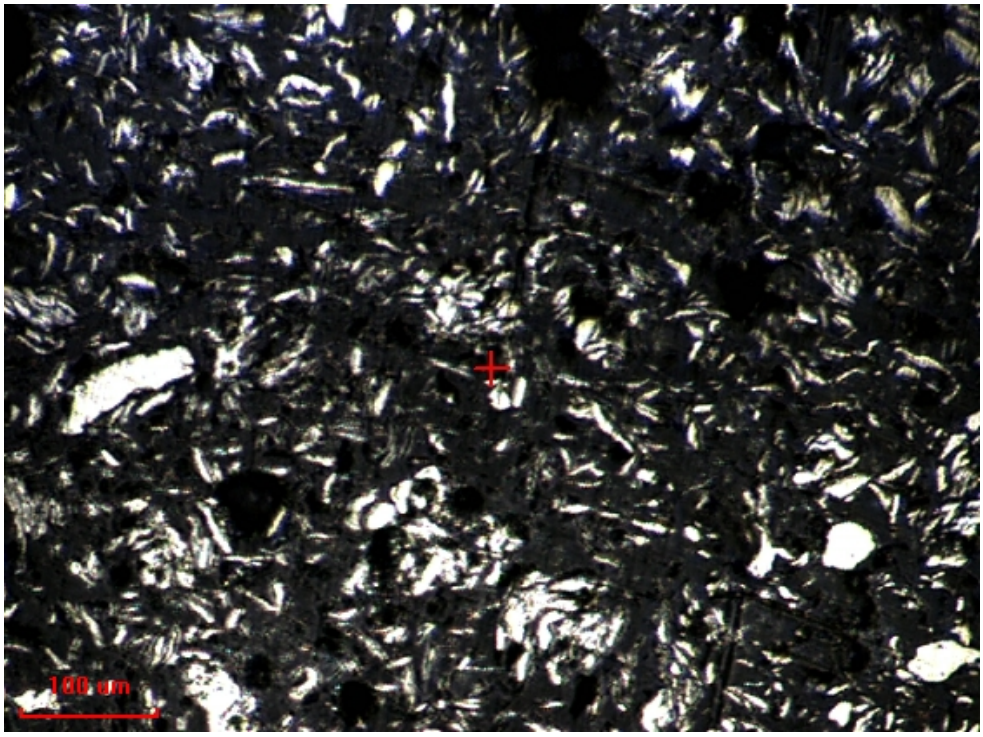

Figure 21. Al – 5 wt.% CNT particles mounted in epoxy matrix viewed at 10x

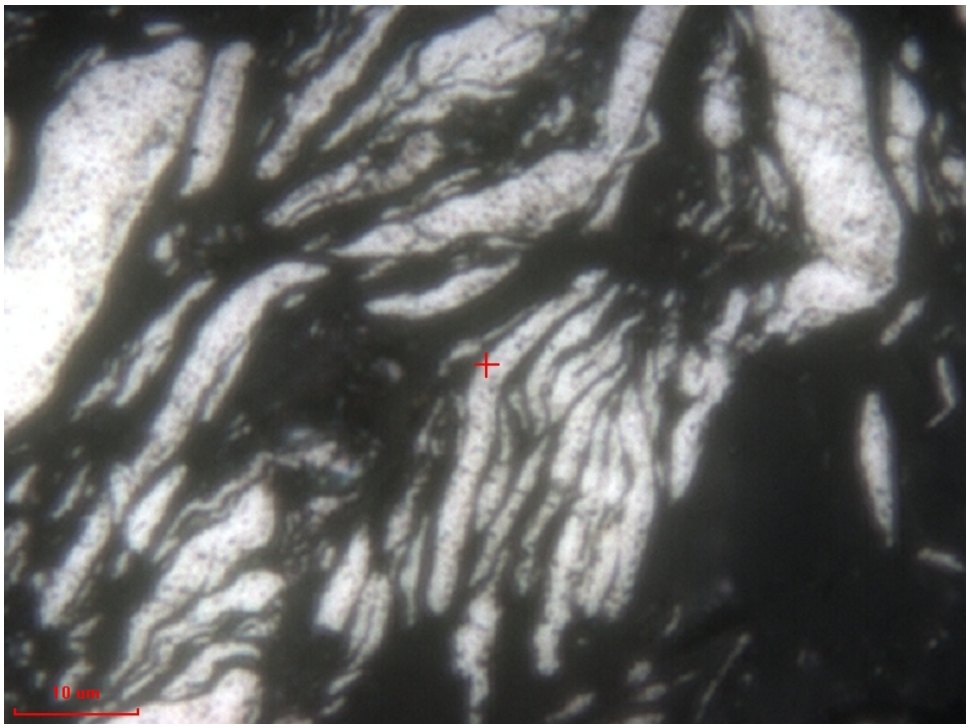

Figure 22. Al – 5 wt.% CNT particles mounted in epoxy matrix viewed at 100x

C. X-RAY DIFFRACTION ANALYSIS FOR GRAIN SIZE AND MICROSTRAIN

X-ray diffraction was used for all MA powders to determine grain size and microstrain. Figure 23 is an XRD spectra plot of one of the composite Al-CNT powders. This plot includes the Cu kalpha2 peaks. Of all the samples made and analyzed using XRD, none showed any noticeable indication of oxide or carbide formation during milling. Only Al peaks were observed, with no other peaks noticeable in the spectra when analyzed at high resolutions.

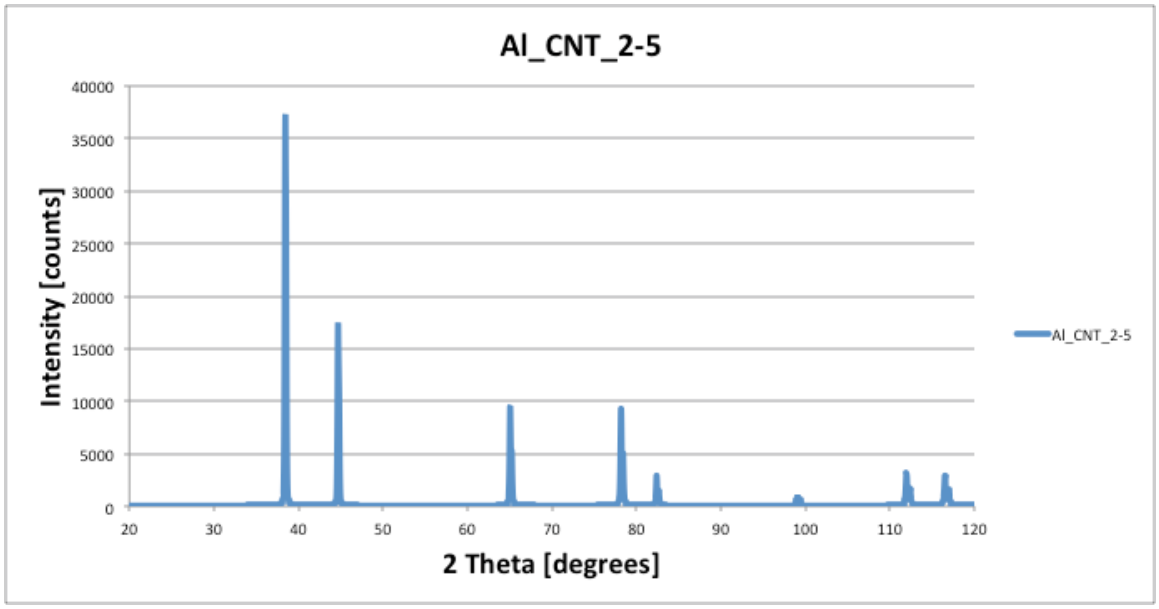

Figure 23. XRD spectra of Al peaks

Grain size and microstrain were calculated for all 27 samples using W-H analysis. Graphs of grain size and microstrain were created based on mill time, percentage of CNT in the Al matrix, and number of run cycles. Of these graphs, certain trends were noticeable in the results. It appears that grain size reduction occurs early in the milling process. Grain sizes of less than 35 nm were calculated in the shortest milling times of six minutes. However, a simplified W-H analysis was used for this calculation, where the integral breadth was the observed breadth minus the instrument broadening. Equation 7 is the more exact equation used for W-H analysis; however, using these terms in the analysis yielded high values for slope (high microstrain) and negative y-intercepts for grain size.

$$\beta = \frac{(\pi * \Gamma)/2}{\eta + (1-\eta) * \sqrt{\pi \ln 2}} \tag{7}$$

Instead of Equation 7, the FWHM calculated by the X'pert software was used instead of using the FWHM as Γ. The instrument broadening data was then subtracted out of the FWHM values. Calculation of grain size and microstrain was then completed using the

simplified method. This method yielded all positive results for grain size (y-intercept) and microstrain (slope). Figure 24 is a W-H analysis plot showing a near linear plot of the data obtained from FWHM values.

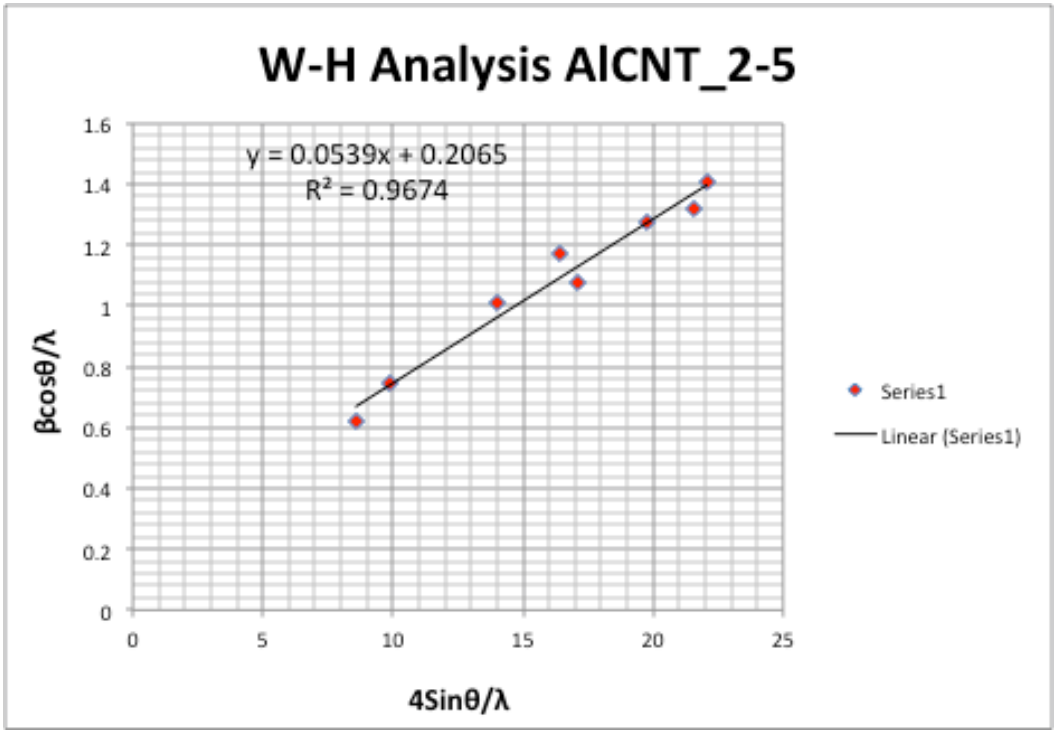

Figure 24. W-H analysis plot for Al 5 wt.% CNT powder milled for 30 minutes total

Two samples from the milling matrix in Section II had the same total milling time but different milling parameters. The first was milled for 6 cycles of 5 min each, and the second 3 cycles of 10 minutes each. W-H analysis for these samples shows very small grain sizes, which push the limits of the W-H analysis but no grain size trends based on different milling conditions that have the same total milling time. Table 7 lists the results for these samples.

	As Received	5 wt% CNT addition	10 wt% CNT addition
30 min [6 cycles * 5 minutes]	1.60	4.84	1.5
30 min [3 cycles * 10 minutes]	7.43	1.28	2.2

Table 7. Grain size in nm for samples milled 30 minutes total

Some samples were milled under various conditions that had similar total milling times. These samples were milled for 12 minutes (6 cycles of 2 minutes), 15 minutes (3 cycles of 5 minutes), and 18 minutes (9 cycles of 2 minutes).

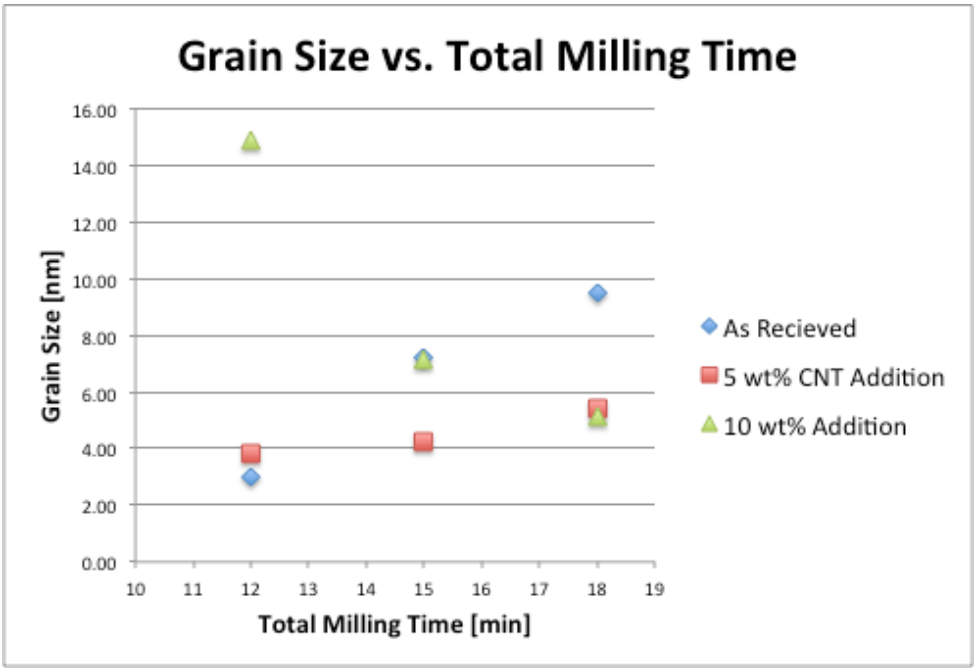

Figure 25. Plot of size vs. total milling time up to 18 minutes

It can be observed from Figure 25 that for the as received powder milled with no addition of CNTs the grain size is increased for longer milling times up to 18 minutes. The opposite is observed in samples containing 10 wt.% additions of CNTs with slight grain size growth during milling. Samples with 5 wt.% CNT show slight growth. Samples containing CNTs that are milled longer than this do not exhibit the same behavior. Essentially, the curve becomes mostly flat for extended milling times.

However, the milled Al powder containing no CNTs exhibits a reduction in grain size for milling extended beyond 18 minutes. This data is shown in Figure 26.

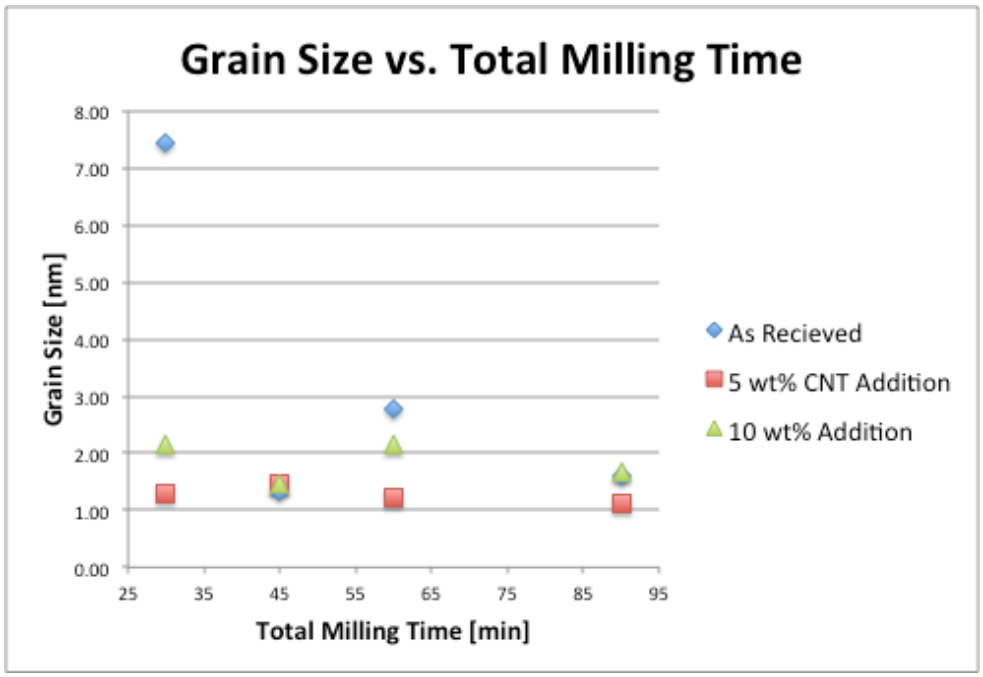

Figure 26. Plot of size vs. total milling time 30 minutes and greater

Plots of strain show some interesting trends as well. Using the same total milling times as the previous charts, there is a small but noticeable increase in microstrain for samples milled between 12 and 15 minutes total. The Al containing no CNTs also exhibits higher microstrain than the samples containing CNTs. Microstrain for samples milled 18 minutes and less are shown in Figure 27 and samples milled for 30 minutes and greater are shown in Figure 28. It appears from these results that microstrain continues to increase for samples milled more than 45 minutes.

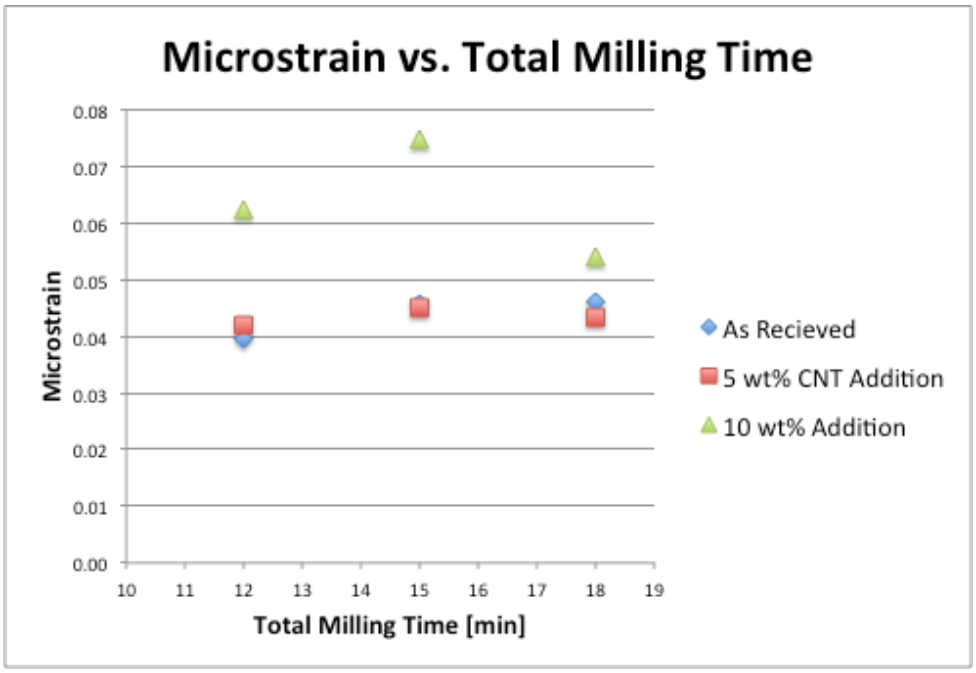

Figure 27. Plot of microstrain vs. total milling time up to 18 minutes

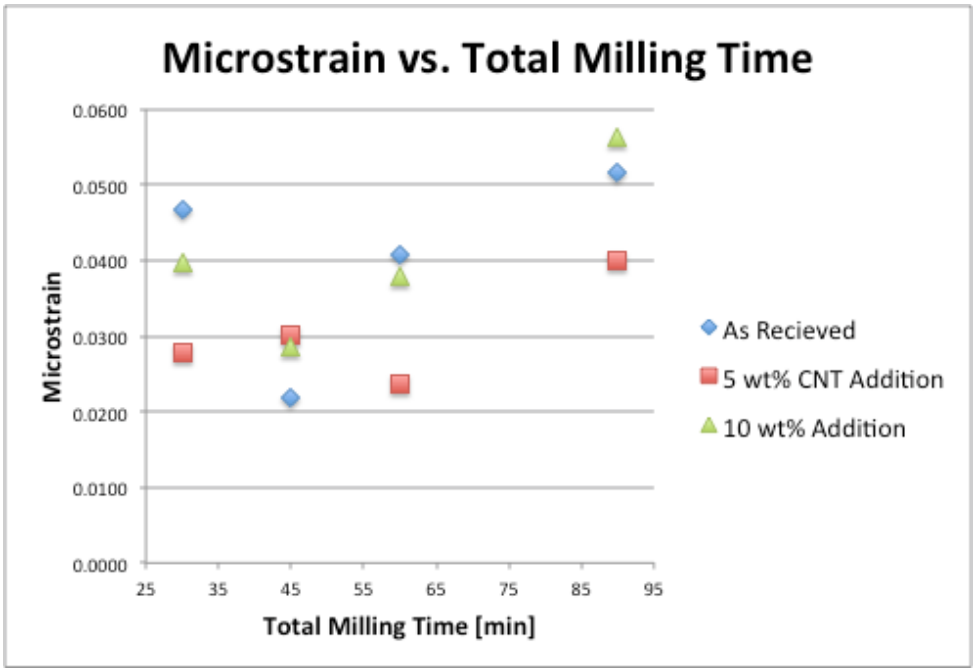

Figure 28. Plot of microstrain vs. total milling time 30 minutes and greater

It appears as though grain size reduction occurs early in the milling process regardless of the combination of run time or number of cycles. These grain size reduction charts show very small nanometer-scale grains, but the results are not verified. Transmission electron microscopy (TEM) is suggested for further analysis of the MA powders for verification and error determination of actual vs. calculated grain size using the W-H method.

D. RAMAN SPECTROSCOPY ANALYSIS

Raman laser spectroscopy provides in indication of the structural integrity of CNTs in the MA powders. Select powders, the same selected for particle size analysis and nanoindentation, were analyzed via this method. The D band originates from wall defects in the CNT structure whereas the G band is ascribed to the in plane vibrations of the honeycomb lattice of the CNTs, e.g., the graphitic structure. The intensity ration between the D and G Raman bands (D/G) can thus be used to evaluate the structural integrity of the sample. Figure 25 shows the Raman spectra of three Al – 5 wt.% powders milled for increasing total times. As can be seen in the figure, the background shows an increase from approximately 1000 counts to 4000 counts between the shortest and longest milled powders. This information suggests that as the powders are being milled for increasing times that the Al is contributing more to the background. This may be an indication of either damage to the CNTs during milling in the form of fracture, or that the CNTs are being forced into the Al matrix particles during longer milling periods. Raman data for Al- 5 wt.% CNT is shown in Figure 29.

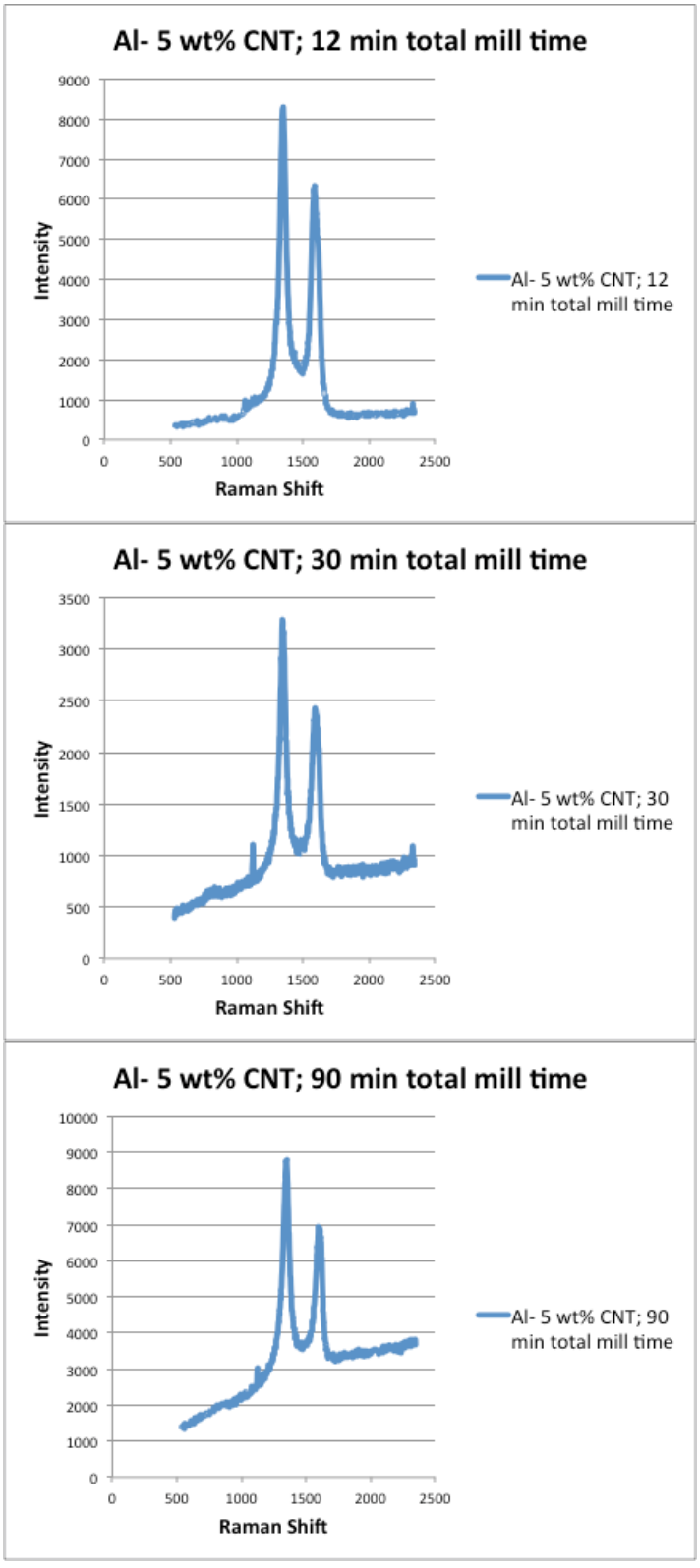

Figure 29. Raman background increase for increased milling time

An increase in background from Al is plausible. Powders milled for increasing milling times tended to visually appear more like Al than have the black color characteristic of CNTs. Figure 30 is an image of the same powders used analyzed in Figure 29. The longest miling time (90 minutes total) has much more of an Al color appearance than the other samples.

Figure 30. Al – 5 wt.% CNT milled for 6, 30, and 90 minutes total

In addition to a comparison of background, the D and G peaks were profile fit and the ratios between them compared. The intensity of the peaks is compared in Figure 33. The D/G ratio of the as-received powder was observed at 1.12. The first and second points on the graph suggest that damage to the CNTs is occurring early in the milling process (less than 30 minutes) and that further milling only slightly increases the amount of damage to the CNTs as the increase between D/G ratios only differs by 0.05 in the last 60 minutes of a 90 minute total mill time.

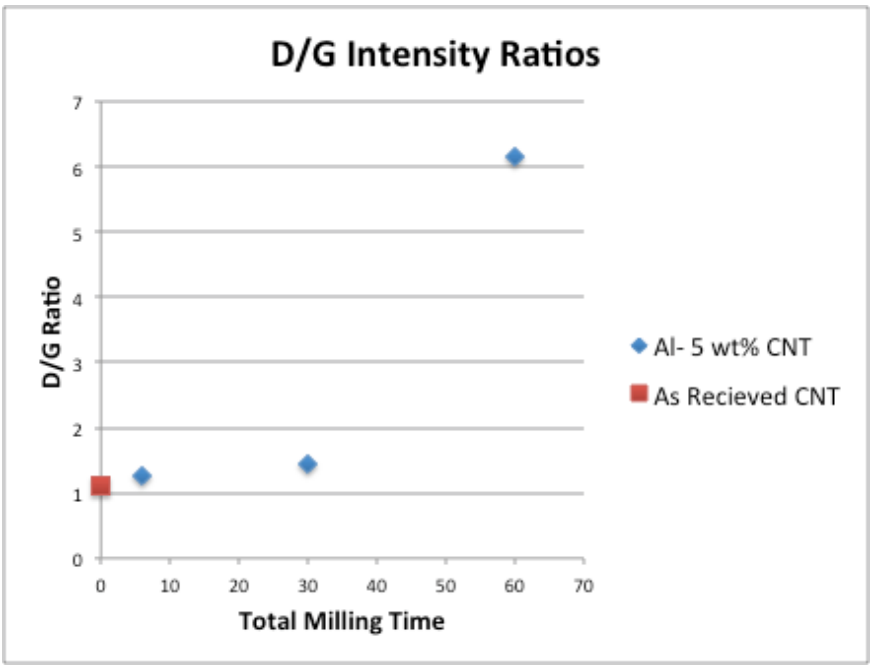

Figure 31. D/G band ratios for as-received and select Al – 5 wt.% powders

E. MECHANICAL PROPERTIES: NANOINDENTATION

Nanoindentation of the same powders analyzed with Raman spectroscopy and laser particle size analysis was also conducted. The polished epoxy pucks containing small amounts of select powders were analyzed for modulus and hardness. The results from these experiments provided inconclusive results. The loading curves for nanoindentation had obvious outliers that were essentially a flat loading curve. These curves were removed from the mean and standard deviation calculations. The results were a slight decrease in modulus, and effectively no change in hardness. These results do not agree with with prior Al-CNT composite studies. Figures 34 and 35 are the mean modulus and hardness graphs created from nanoindentation data. Some of these results had very high standard deviations of over 30 percent.

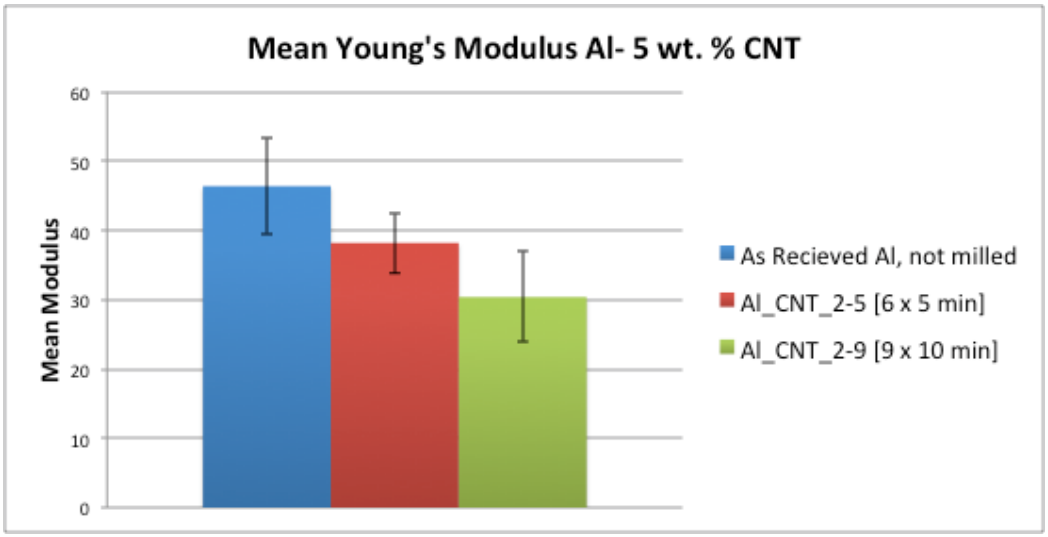

Figure 32. Mean Young's modulus for select Al – 5 wt.% CNT samples

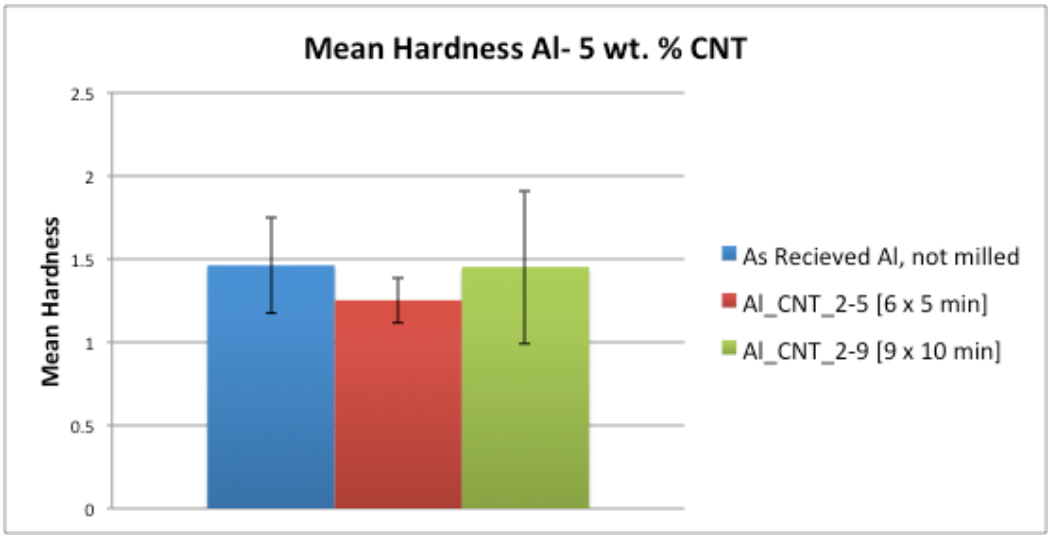

Figure 33. Mean hardness for select Al – 5 wt.% CNT samples

The likely cause of the high range of standard deviation and inconsistent modulus and hardness values may be a sample mechanical compliance issue. A large mechanical compliance will lead to a significant underestimate of the measured material's elastic modulus. Particularly for milled powder, there is substantial uncertainty about the thickness of the Al composite material underneath the indenter tip. This uncertainty makes it difficult to account for the compliance of the epoxy substrate. Typical values

for the Young's modulus of Al are 69–74GPa, not the 40Gpa or less observed here [29]. Future work will examine the role of this epoxy compliance and how to account for it correctly.

THIS PAGE INTENTIONALLY LEFT BLANK

IV. CONCLUSIONS

Al-CNT composites were successfully synthesized using cryogenic milling. W-H analysis of the resultant powders shows a rapid decrease in grain size of the composite. This decrease in grain size seems to occur early in the milling process. These results should now be verified using TEM. The grain sizes are all under 35 nm for all samples, with many samples having grain sizes of approximately 2 nm. The analysis conducted using W-H method is certainly at the lower bound of the method and using TEM will uncover any errors in the analysis.

Grain size reduction seems to occur early in the milling process. After 18 minutes of milling all samples had grain sizes of less than 10 nm, with most of them less than 5 nm. Milling greater than 20–30 minutes seems to have no effect on grain size reduction. However, this may be a factor in dispersion of CNTs in the matrix.

Milling parameters such as number of cycles and cycle run time do not seem to make a noticeable difference in grain size reduction. A comparison of total milling time seems to be better as no useful data is apparent from the varied number of cycles and run times.

There is likely some residual strain after the milling process of the Al-CNT powders. The noticeable shift to the right in the peak width curves, and data showing continuously increasing strain for after 45 minutes of milling from W-H analysis suggest residual strain in the composites.

Dispersion of CNTs in the Al matrix is not fully known using the methods in this study. Optical methods used were not of high enough resolution to view and assess the CNT dispersion. Both 5 and 10 wt.% CNT powders exhibited a more Al-like appearance as milling time increased. This may be due to the CNTs being pushed in to the Al matrix during milling or damage occurring to the CNTs. SEM analysis is recommended to further assess the condition and dispersion of CNTs in the composite powders.

Analysis of the D and G band ratios using Raman spectroscopy shows that some damage to the CNTs may be occurring. The ratios in comparison to total milling time

suggest that most damage is occurring during the first 30 minutes of milling. Milling in excess of 30 minutes seems to further damage the CNTs, but not on the same scale that occurs early in the milling process. SEM analysis is recommended to further study CNT condition in the Al matrix.

Average particle size does not change significantly for any of the total milling times used in this study. However, the distribution of larger size particles is noticed for powders that are milled for long durations. There is a noticeable shift in the distribution curve showing this.

Mechanical properties from nanoindentation are inconclusive. Both elastic modulus and hardness data showed a wide range with large standard deviations. This is likely due to the method of mounting the powders in epoxy and not knowing the orientation of the particles selected for nanoindentation.

LIST OF REFERENCES

[1] A. Ramasamy, A. M. Hill, A. E. Hepper, A. M. J. Bull, and J. C. Clasper, "Blast mines: Physics, injury mechanisms and vehicle protection," *Journal of the Royal Army Medical Corps*, vol. 155, no. 4, pp. 258–264, 2009.

[2] T. V. Brook, "MRAPs can't stop newest weapon" [Internet]. http://www.usatoday.com/news/world/iraq/2007-05-31-mrap-insurgents_N.htm. July 15, 2007 [Mar. 22, 2012].

[3] A. A. Baker, D. M. Braddick, and P. W. Jackson, "Fatigue of boron-aluminum and carbon-aluminum fiber composites," *Journal of Materials Science*, vol. 7, no. 7, pp. 747–762, 1972.

[4] E. D. Lamotte, E. K. Phillips, A. J. Perry, and H. R. Killias, Continuously cast aluminum-carbon fiber composites and their tensile properties," *Journal of Materials Science*, vol. 7, no. 3, pp. 346–348, 1972.

[5] S. R. Bakshi, D. Lahiri, and A. Agarwal, "Carbon nanotube reinforced metal matrix composites – A review," *International Materials Reviews*, vol. 55, no. 1, pp. 41–64, 2010.

[6] B. Sneed, "Synthesis and characterization of al-nanodiamond composite powders by high-energy ball milling." M.S. thesis, Naval Postgraduate School, Monterey, CA, 2011.

[7] I. A. Ibrahim, F. A. Mohamed, and E. J. Lavernia, "Particulate reinforced metal matrix composites—a review," *Journal of Materials Science*, vol. 26, no. 5, pp. 1137–1156, 1991.

[8] A. M. K. Esawi, K. Morsi, A. Sayed, A. A. Gawad, and P. Borah, "Fabrication and properties of dispersed carbon nanotube–aluminum composites," *Materials Science and Engineering A*, vol. 508, no. 1–2, pp. 167–173, 2009.

[9] M. Huller, G. Chernik et al, "Mechanical alloying in planetary mills of high accelerations," *Rev. Adv. Mater. Sci.*, vol. 18, pp. 366–374, 2008.

[10] M. Myers and K. Chawla, "Grain Boundaries in Plastic Deformation (Grain-Size Strengthening)," in *Mechanical Behavior of Materials, 2*nd ed., Cambridge, UK, Cambridge Univ. Press, 2009, ch. 5, sec. 4, pp. 345–351, 774–783.

[11] T. Kuzumaki, K. Miyazawa, H. Ichinose, and K. Ito, "Processing of carbon nanotube reinforced aluminum composite," *Journal of Materials Research*, vol. 13, no. 9, pp. 2445–2449, 1998.

[12] R. George, K. Kashyap, R. Rahul, and S. Yamdagni, "Strengthening in carbon nanotube/aluminium (CNT/Al) composites," *Scripta Materialia*, vol. 53, no. 10, pp. 1159–1163, 2005.

[13] H. Kwon, M. Estili, K. Takagi, T. Miyazaki, and A. Kawasaki, "Combination of hot extrusion and spark plasma sintering for producing carbon nanotube reinforced aluminum matrix composites," *Carbon*, vol. 47, no. 3, pp. 570–577, 2009.

[14] S. Cho, K. Kikuchi, T. Miyazaki, K. Takagi, A. Kawasaki, and T. Tsukada, "Multiwalled carbon nanotubes as a contributing reinforcement phase for the improvement of thermal conductivity in copper matrix composites," *Scripta Materialia*, vol. 63, no. 4, pp. 375–378, 2010.

[15] S. C. Tjong and H. Chen, "Nanocrystalline materials and coatings," *Materials Science and Engineering: R: Reports*, vol. 45, no. 1–2, pp. 1–88, 2004.

[16] T. Laha and A. Agarwal, "Effect of sintering on thermally sprayed carbon nanotube reinforced aluminum nanocomposite," *Materials Science and Engineering A*, vol. 480, no. 1-2, pp. 323–332, 2008.

[17] C. C. Koch, "Synthesis of Nanostructured Materials by Mechanical Milling: Problems and Opportunities," *Nanostructured Materials*, vol. 9, pp. 13–22, 1997.

[18] S. Bakshi, V. Singh, K. Balani, D. Mccartney, S. Seal, and A. Agarwal, "Carbon nanotube reinforced aluminum composite coating via cold spraying," *Surface and Coatings Technology*, vol. 202, no. 21, pp. 5162–5169, 2008.

[19] C. C. Koch, "Nanocrystalline powder consolidation methods," in *Nanostructured Materials: Processing, Properties and Potential Applications*, Norwich, NY: William Andrew Pub. 2002, ch. 4, sec. 3, pp. 155–156.

[20] H. Assadi, F. Gärtner, T. Stoltenhoff, and H. Kreye, "Bonding mechanism in cold gas spraying," *Acta Materialia*, vol. 51, no. 15, pp. 4379–4394, 2003.

[21] C. Suryanarayana, "Mechanical alloying and milling," *Progress in Materials Science*, vol. 46, no. 1–2, pp. 1–184, 2001.

[22] C. DeCastro and B. Mitchell, "Nanoparticles from Mechanical Attrition," in *Synthesis, Functionalization and Surface Treatment of Nanoparticles*, M. Baraton, Ed. Valencia, CA: American Scientific Publishers, 2002, pp 1–15.

[23] A. Calka and J. I. Nikolov, "The Dynamics of Magneto-Ball Milling and its Effects on Phase Transformations During Mechanical Alloying," *Materials Science Forum* vol. 179–181, pp. 333–338, 1995.

[24] G. M. Wang, S. J. Campbell, A. Calka, and W. A. Kaczmarek, "Synthesis and structural evolution of tungsten carbide prepared by ball milling," *Journal of Materials Science*, vol. 32, no. 6, pp. 1461–1467, 1997.

[25] S. Mørup, J. Z. Jiang, F. Bødker, and A. Horsewell, "Crystal growth and the steady-state grain size during high-energy ball-milling," *Europhysics Letters*, vol. 56, no. 3, pp. 441–446, 2001.

[26] L. Ajdelsztajn, et al, "Cold spray deposition of nanocrystalline aluminum alloys," *Metallurgical and Materials Transactions*, vol. 36A, no. 3, pp. 657–666, 2005.

[27] G. Goncales, D. Oleszak, A. Sagarzazu, R. Villalba, and L. D'Onofrio, "Mechanical alloying of FeCoCr," *Revista Latinoamericana de Metalurgia y Materiales*, vol. 36, no. 1, pp. 64–70, 2011.

[28] Horiba, Inc. "High performance laser diffraction particle size analyzer." [Internet]. http://www.horiba.com/scientific/products/particle-characterization/particle-size-analysis/details/la-950-108/, [Mar. 24, 2012].

[29] W. C. Oliver, G. M. Pharr, "An improved technique for determining hardness and elastic modulus using load and displacement sensing indentation experiments," J. *Mater. Res.* 7, pp. 1564–1583, 1992.

THIS PAGE INTENTIONALLY LEFT BLANK

INITIAL DISTRIBUTION LIST

1. Defense Technical Information Center
   Ft. Belvoir, Virginia

2. Dudley Knox Library
   Naval Postgraduate School
   Monterey, California